
Citation:

Perepelkin, NV and Kovalev, AE and Gorb, SN and Borodich, FM (2019) Estimation of the elastic modulus and the work of adhesion of soft materials using the extended Borodich–Galanov (BG) method and depth sensing indentation. *Mechanics of Materials*, 129. pp. 198-213. ISSN 0167-6636
DOI: <https://doi.org/10.1016/j.mechmat.2018.11.017>

Link to Leeds Beckett Repository record:

<https://eprints.leedsbeckett.ac.uk/id/eprint/6684/>

Document Version:

Article (Accepted Version)

Creative Commons: Attribution-Noncommercial-No Derivative Works 4.0

The aim of the Leeds Beckett Repository is to provide open access to our research, as required by funder policies and permitted by publishers and copyright law.

The Leeds Beckett repository holds a wide range of publications, each of which has been checked for copyright and the relevant embargo period has been applied by the Research Services team.

We operate on a standard take-down policy. If you are the author or publisher of an output and you would like it removed from the repository, please [contact us](#) and we will investigate on a case-by-case basis.

Each thesis in the repository has been cleared where necessary by the author for third party copyright. If you would like a thesis to be removed from the repository or believe there is an issue with copyright, please contact us on openaccess@leedsbeckett.ac.uk and we will investigate on a case-by-case basis.

1 Estimation of the elastic modulus and the work of
2 adhesion of soft materials using the extended
3 Borodich-Galanov (BG) method and depth sensing
4 indentation

5 Nikolay V. Perepelkin^{a,c,*}, Alexander E. Kovalev^b, Stanislav N. Gorb^b,
6 Feodor M. Borodich^a

7 ^a*School of Engineering, Cardiff University, Cardiff, CF24 3AA, UK*

8 ^b*Department of Functional Morphology and Biomechanics, Zoological Institute of the
9 University of Kiel, Am Botanischen Garten 1-9, D-24098, Kiel, Germany*

10 ^c*Department of Applied Mathematics, National Technical University "Kharkiv
11 Polytechnic Institute", 2 Kyrpychova Str, Kharkiv, 61002, Ukraine*

12 **Abstract**

13 The depth-sensing indentation (DSI) is currently one of the main experimen-
14 tal techniques for studying elastic properties of materials of small volumes.
15 Usually DSI tests are performed using sharp pyramidal indenters and the
16 load-displacement curves obtained are used for estimations of elastic mod-
17 uli of materials, while the curve analysis for these estimations is based on
18 the assumptions of the Hertz contact theory of non-adhesive contact. The
19 Borodich-Galanov (BG) method provides an alternative methodology for es-
20 timations of the elastic moduli along with estimations of the work of adhesion
21 of the contacting pair in a single experiment using the experimental DSI data
22 for spherical indenters. The method assumes fitting the experimental points
23 of the load-displacement curves using a dimensionless expression of an appro-
24 priate theory of adhesive contact. Earlier numerical simulations showed that
25 the BG method was robust. Here first the original BG method is modified
26 and then its accuracy in the estimation of the reduced elastic modulus is
27 directly tested by comparison with the results of conventional tensile tests.

28 The method modification is twofold: (i) a two-stage fitting of the theoret-
29 ical DSI dependency to the experimental data is used and (ii) a new objective
30 functional is introduced which minimizes the squared norm of difference be-
31 tween the theoretical curve and the one used in preliminary data fitting. The
32 direct experimental validation of accuracy and robustness of the BG method

has two independent steps. First the material properties of polyvinyl siloxane (PVS) are determined from a DSI data by means of the modified BG method; and then the obtained results for the reduced elastic modulus are compared with the results of tensile tests on dumbbell specimens made of the same charge of PVS.

Comparison of the results of the two experiments showed that the absolute minimum in relative difference between individual identified values of the reduced elastic modulus in the two experiments was 3.80%; the absolute maximum of the same quantity was 27.38%; the relative difference in averaged values of the reduced elastic modulus varied in the range 16.20 ... 17.09% depending on particular settings used during preliminary fitting. Hence, the comparison of the results shows that the experimental values of the elastic modulus obtained by the tensile tests are in good agreement with the results of the extended BG method. Our analysis shows that unaccounted factors and phenomena tend to decrease the difference in the results of the two experiments. Thus, the robustness and accuracy of the proposed extension of the BG method has been directly validated.

Keywords: the BG method, estimation of material properties, depth sensing indentation, tensile testing, polyvinyl siloxane (PVS)

1. Introduction

Evaluation of elastic moduli of materials and their adhesive properties is one of the important tasks of modern materials science. However, the experimental estimations of the material properties become particularly challenging if the specimen is made of a small quantity of material or if it is a thin film deposited on the surface of another object. In these cases one of the most useful techniques is the depth sensing indentation (DSI). This technique includes loading and unloading of a material specimen by a probe (indenter), and continuous monitoring the value of the applied force (P) and the probe displacement (δ).

DSI was introduced by Kalei (1968) 50 years ago. Then it was suggested to use the experimental unloading $P - \delta$ curves for extracting the values of the elastic modulus of the tested material (Bulychev et al., 1975, 1976; Shorshorov et al., 1981). Currently there are several approaches for evaluation of the elastic modulus employing the DSI experiments with sharp pyramidal indenters (Doerner and Nix, 1986; Oliver and Pharr, 1992; Bull,

2005; Galanov and Dub, 2017). On the other hand, the DSI technique works with spherical indenters too. One of the techniques based on an inverse analysis of the DSI experiments with spherical indenters is the BG method. Originally the BG method was introduced by Borodich and Galanov (2008) and then it was discussed in a series of papers (Borodich et al., 2012a,b, 2013). Numerical tests and experimental studies showed that even the original BG method is simple and robust. Our paper is devoted to the extension of the BG method and direct experimental validation of both the accuracy and robustness of this extended method.

To explain the advantages of the BG approach, we need to discuss the common DSI techniques working with pyramidal indenters first. In the above cited approaches to DSI by sharp indenters, the unknown elastic properties of samples are estimated from the experimental DSI data by solving an inverse problem to the non-adhesive Hertz-type contact problem (see e.g., Johnson (1985); Popov (2010); Borodich (2014)). As any other model-based approaches, it requires a prebuilt mathematical model of the interaction between the probe and the specimen. It follows from the Hertz contact theory that the elastic modulus may be estimated using the BASH (Bulychev–Alekhin–Shorshorov) formula. Originally formula was derived for frictionless contact of some axisymmetric punches and it was suggested to extend it to non-axisymmetric indenters, e.g. pyramidal indenters (Bulychev et al., 1975). Then it was noted that if one applies the geometrically linear formulation of Hertz-type contact problem to unloading branch of the $P - \delta$ curve then one needs to take into account the actual distance between the indenter and the plastically distorted surface (the Galanov effect) (Galanov et al., 1983, 1984). It was also shown that the friction between the indenter and the specimen surface may also affect the slope of the unloading curve (Borodich and Keer, 2004b). Thus, the BASH formula can be written as (Argatov et al., 2017)

$$\frac{dP}{d\delta} = \beta \frac{2}{\sqrt{\pi}} E^* \sqrt{A}, \quad \beta = \beta_1 \cdot \beta_2 \cdot \beta_3 \quad (1)$$

where A is the area of the contact region and E^* is the reduced elastic contact modulus. For isotropic materials, this modulus can be obtained from the following formula

$$\frac{1}{E^*} = \frac{1 - \nu_1^2}{E_1} + \frac{1 - \nu_2^2}{E_2}$$

where E_i and ν_i ($i = 1, 2$) are the elastic modulus and Poisson's ratio of the two contacting solids (the specimen and the indenter) respectively. If the

indenter is rigid, i.e. $E_2 = \infty$ then $E^* = E/(1-\nu^2)$ where $E = E_1$ and $\nu = \nu_1$ are the elastic modulus and Poisson's ratio of the half-space, respectively. In (1) the factor β_1 is introduced due to the concept of the effective indenter shape (the Galanov effect) (Galanov et al., 1983, 1984), β_2 is the contact area shape factor which extends the BASH formula to the non-axisymmetric case, and the factor β_3 is introduced due to the effects of friction between the indenter and the half-space (Borodich and Keer, 2004a,b). It has been shown in the case of adhesive (no-slip) contact between a rigid indenter and an elastic sample $\beta_3 = C_{NS}$ that can be expressed as a function of the material Poisson ratio (ν)

$$C_{NS} = \frac{(1 - \nu) \ln(3 - 4\nu)}{1 - 2\nu}. \quad (2)$$

The above described approaches to indentation by sharp indenters have several drawbacks. Strictly speaking the Hertz contact theory is not applicable to these tests based on the use of sharp indenters (see a discussion in Borodich and Keer (2004a); Chaudhri and Lim (2007); Borodich (2014)), in addition, it ignores the adhesive effects between the indenter and the sample. On the other hand, the use of spherical indenters allows the researchers to avoid plastic deformations of specimens and therefore, they may work in the framework of theory of elasticity and do not violate the geometrical assumptions of the Hertz formulation. In addition, devices with cantilever-supported indenters may be used. In the case of cantilever support the unavoidable inclination of the cantilever (see e.g. Al-Musawi et al. (2016)) has much less influence on interaction between the indenter and the specimen in comparison to the case when a sharp indenter is used.

The original version of the BG method is based on solving an inverse problem to adhesive contact between a spherical indenter and an elastic half-space using one of the well-established theories of adhesive contact, e.g. the JKR or DMT ones. The method uses a dimensionless mathematical dependency between the force applied to the indenter and its displacement (the theoretical load-displacement curve) as the mathematical model of the adhesive interaction "indenter-specimen".

Any analytical force-displacement dependency can be written in a dimensionless form. To do so, one needs to determine the so-called characteristic scales of the problem. These scales are the model parameters and their values are subject to adjustment through an optimization process until the best fit

of the theoretical curve to the experimental data points is found. The particular representation of the theoretical curve and the characteristic scales depends on the theory of adhesive contact chosen as the framework of the problem (e.g. the Johnson-Kendall-Roberts (JKR)(Johnson et al., 1971) or the Derjaguin-Muller-Toporov (DMT)(Derjaguin et al., 1975) theories). For example, for a spherical indenter of radius R , the characteristic scales may be taken as

$$P_c = \frac{3}{2}\pi w R, \quad \delta_c = \frac{3}{4} \left(\frac{\pi^2 w^2 R}{E^{*2}} \right)^{1/3}. \quad (3)$$

In the JKR theory, the above characteristic scales have a clear mechanical meaning: P_c is denoted the absolute value of the pull-off force, and δ_c is the absolute value of the minimum displacement that occurs due to adhesion. Once optimal values of P_c and δ_c are found, the material properties E^* and w can be easily evaluated by inversion of the latter formulae

$$w = \frac{2P_c}{3\pi R}, \quad E^* = \frac{P_c}{4} \sqrt{\frac{3}{R\delta_c^3}}. \quad (4)$$

Contrary to the interpretation of the DSI tests based on the BASH formula, the BG method allows not only to evaluate the elastic properties (the reduced elastic contact modulus E^*) but also the adhesive properties (the work of adhesion w) of tested pair of materials. Unlike the other methods of mechanics of materials that require separate experimental set-ups for the determination of elastic and adhesive properties of materials, the BG method allows to identify those quantities simultaneously using a single set-up. Moreover, it can utilize only the stable compressive part of the load-displacement data whereas some other approaches require the pull-off force measurements in order to estimate the value of the work of adhesion (e.g. Ebenstein and Wahl (2006); Carrillo et al. (2005); Rundlöf et al. (2000); Wahl et al. (2006); Yu et al. (2015)). However, measurements of the pull-off force can be influenced by many factors: the roughness of contacting surfaces, surface chemistry, wear of the DSI probe, chemical modification of its surface (in case of atomic force microscopy used), dust particles etc. (see e.g., Grierson et al. (2005); Beach et al. (2002); Gorb and Gorb (2009)). Therefore, the tensile part of DSI load-displacement data can be considered unstable and less trustworthy, and the BG method has an advantage here.

The BG method is non-direct because the characteristic values are not measured but rather evaluated from the stable part of the $P - \delta$ diagram,

164 while P_c is extracted from measurements on the unstable part of the dia-
 165 gram in the direct methods (Wahl et al., 2006; Ebenstein and Wahl, 2006).
 166 In addition, the BG method differs from the ordinary least-squares fitting
 167 because: (i) it uses different objective functional and therefore, it provides
 168 different optimum, (ii) whenever possible, dimensionless variables are used
 169 which allows to apply optimization procedures to the quantities of different
 170 physical nature and different orders of magnitude.

171 The paper is organized as follows. In Section 2, the paradigm of the BG
 172 method is extended. Originally the method was applied only to the con-
 173 tact problem between a spherical indenter and an elastic half-space. Here,
 174 it is argued that the BG method can be considered as a general model-
 175 based approach to determination of the effective contact modulus and the
 176 work of adhesion of materials or structures from the DSI data. Examples
 177 of appropriate theories of adhesive contact and the corresponding theoret-
 178 ical load-displacement curves are considered. Then an alternative formula-
 179 tion of the objective functional of the BG method is also given. A concept
 180 of two-stage fitting of the theoretical DSI dependency to the experimental
 181 data points is introduced. This means that the data is fitted firstly by an
 182 auxiliary curve which acts as a filter in certain sense. The mathematical
 183 representation of that pre-fitting curve is supposed to be as simple as pos-
 184 sible. This allows one to use some advanced fitting/filtering techniques to
 185 reduce measurement noise and fluctuations in the data. Secondly, the the-
 186 oretical load-displacement curve (the expected DSI dependency which may
 187 be a complex expression) is fitted to the auxiliary one via minimization of
 188 the squared norm of the difference of the two functions (the objective func-
 189 tional). The sought material properties are determined from the optimal set
 190 of characteristic parameters that give minimum to the objective functional.

191 In Section 3 the results of a DSI-based experiment and an application of
 192 the extended BG method are described. The experimental set-up and raw
 193 data pre-processing are also discussed. A specimen was made of polyvinyl
 194 siloxane (PVS). This is an elastomer widely used as an impression material,
 195 particularly in dentistry. A series of DSI tests was carried out using DSI
 196 equipment and a spherical indenter (lens) of large radius ($R = 5.155$ mm)
 197 supported by a cantilever spring with constant $c = 1023.9$ N/m. The experi-
 198 mental data was processed using the extended BG method, and the values of
 199 the modulus E^* and the work of adhesion w were calculated. The specimen
 200 size was large enough to consider it as an elastic half-space, and therefore,
 201 the JKR theory of adhesive contact was applied.

202 In Section 4 the description of the tensile set-up used for the validation of
 203 the BG method is given as well as the discussion regarding post-processing
 204 of the measured data and the obtained results. In this experiment we per-
 205 formed conventional tensile testing (Davis, 2004) of ISO 37 type 3 dumbbell
 206 specimens made of exactly the same PVS material using Zwick Roell ten-
 207 sile machine. As the result of this experiment, the elastic modulus E and
 208 Poisson's ratio ν were determined which allowed us to calculate the reduced
 209 elastic contact modulus $E^* = E/(1 - \nu^2)$ and compare it to the value ob-
 210 tained using the BG method. Since our piece of equipment was not equipped
 211 with extensometer, two types of mathematical modelling (analytical and fi-
 212 nite element) of the tensile experiment was used to introduce correction into
 213 the values of E produced from the raw tensile data. The value of Poisson's
 214 ratio was estimated from video records of stretching process by using the
 215 methods of photogrammetry.

216 In Section 5, the results of the two experiments are compared and the used
 217 approaches discussed. It is shown that the values of E^* calculated using the
 218 two different approaches coincide well. Our analysis shows that unaccounted
 219 factors and phenomena tend to decrease the difference in the results of the
 220 two experiments. Thus, the accuracy of the BG method has been directly
 221 validated in this work. The obtained results also provide more experimen-
 222 tal data on PVS properties, since this matter is not widely represented in
 223 literature (see e.g., Chai et al. (1998); Wieckiewicz et al. (2016))

224 2. The extended BG method

225 As it is mentioned above, the BG method allows one to extract from the
 226 experimental data of DSI test the two properties of the tested material simul-
 227 taneously: the reduced elastic contact modulus E^* and the work of adhesion
 228 w . The BG method in its original form presumes the use of either the JKR
 229 or the DMT theories of adhesive contact between a spherical indenter and
 230 an elastic half-space. The load-displacement relation in these theories can be
 231 represented in the dimensionless form as

$$F\left(\frac{P}{P_c}, \frac{\delta}{\delta_c}\right) = 0. \quad (5)$$

232 Let us consider a set of N measured experimental values of indentation
 233 depth δ_i and indentation force $P_i : (\delta_i, P_i)$, $i = 1, \dots, N$. If the measurements
 234 are absolutely exact, then the values of P_c and δ_c can be determined quite

235 easily. Indeed, the theoretical curve in such case passes through all the data
 236 points which can be mathematically expressed as the set of equalities

$$F\left(\frac{P_i}{P_c}, \frac{\delta_i}{\delta_c}\right) = 0, \quad i = 1, \dots, N. \quad (6)$$

237 The correct values of P_c and δ_c make all of these equations valid simultane-
 238 ously. Therefore, one needs to take any two of them and solve for P_c and
 239 δ_c . However, the real experimental measurements (δ_i, P_i) always contain some
 240 measurement errors. Therefore, one needs to take into account all of the N
 241 expressions in (6) simultaneously. Due to measurement errors the expres-
 242 sions (6) never become true at the same time and the inverse problem of
 243 finding the characteristic scales from the DSI data is ill-defined (one has an
 244 overdetermined system of equations) (Borodich and Galanov, 2008).

245 Since it is impossible to make all of the expressions in (6) true, one
 246 can only minimize the measure of the overall 'error' produced in (6). If
 247 $\varepsilon_i = F\left(\frac{P_i}{P_c}, \frac{\delta_i}{\delta_c}\right)$ is the residual of i -th equation, then the measure of the
 248 total 'error' can be the mean square value of all such residuals

$$\epsilon = \frac{1}{N} \sum_{i=1}^N \varepsilon_i^2. \quad (7)$$

249 Hence, in order to find the appropriate values of the characteristic pa-
 250 rameters an optimization problem must be solved. The optimal values of the
 251 characteristic parameters P_c^*, δ_c^* that minimize the mean square residual (7)
 252 of the equations (6) are found as the result of minimization of the objective
 253 functional (the cost functional) of the problem $\Phi(P_c, \delta_c)$

$$\{P_c^*, \delta_c^*\} = \arg \min \Phi(P_c, \delta_c) \quad (8)$$

254 where

$$\Phi(P_c, \delta_c) = \sum_{i=1}^N \left[F\left(\frac{P_i}{P_c}, \frac{\delta_i}{\delta_c}\right) \right]^2. \quad (9)$$

255 After the above optimization problem is solved (see e.g., Boyd and Vanden-
 256 berghe (2004); Chong and Zak (2001)), the theoretical curve (5) becomes best
 257 fit to the experimental data in the sense of (9) through the choice $P_c = P_c^*$
 258 and $\delta_c = \delta_c^*$ and the sought material parameters E^* and w can be evaluated
 259 using (4).

260 In particular, if the JKR theory of adhesive contact (Johnson et al., 1971)
 261 is used, then the load-displacement dependency can be written as a piece-wise
 262 function of the form

$$\left\{ \begin{array}{l} (3\chi - 1) \left(\frac{1 + \chi}{9} \right)^{\frac{1}{3}} - \frac{\delta}{\delta_c} = 0 \\ \text{for } \chi \geq 0, \frac{\delta}{\delta_c} \geq -3^{-2/3}, \\ \\ (3\chi + 1) \left(\frac{1 - \chi}{9} \right)^{\frac{1}{3}} - \frac{\delta}{\delta_c} = 0 \\ \text{for } \frac{2}{3} \geq \chi \geq 0, -3^{-2/3} > \frac{\delta}{\delta_c} \geq -1 \end{array} \right. \quad (10)$$

263 where $\chi = \sqrt{1 + \frac{P}{P_c}}$ (Maugis, 2000). As mentioned earlier, the characteristic
 264 scales P_c and δ_c are expressed as (3) for spherical indenter.

265 The experimental data is fitted with the stable part of the above depen-
 266 dency which becomes the function $F\left(\frac{P}{P_c}, \frac{\delta}{\delta_c}\right)$ in the BG method:

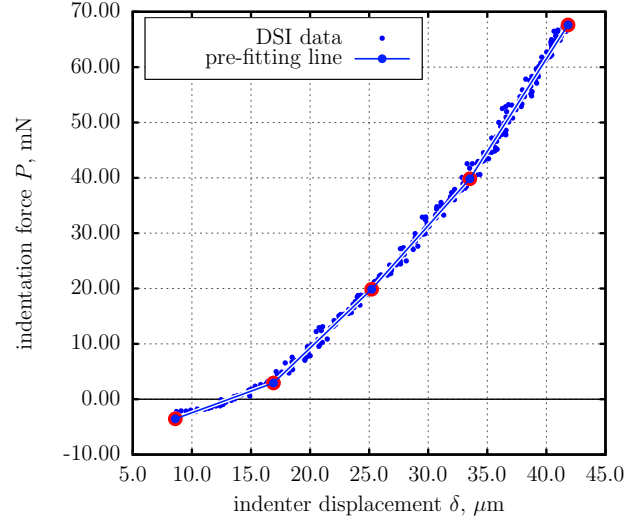
$$F\left(\frac{P}{P_c}, \frac{\delta}{\delta_c}\right) = (3\chi - 1) \left(\frac{1 + \chi}{9} \right)^{\frac{1}{3}} - \frac{\delta}{\delta_c} = 0. \quad (11)$$

267 As compared to the fitting approaches used by other researchers, the BG
 268 method (8)-(9) has its own distinctive features: (i) the metric (9) differs
 269 from the one normally introduced in least-squares curve fitting, therefore
 270 producing different optimum point, (ii) the method uses fitting curve writ-
 271 ten in dimensionless form which allows to treat quantities of different orders
 272 of magnitude in the same way, (iii) the fitting process is performed via ad-
 273 justing characteristic scales P_c and δ_c and not the material properties. Also
 274 the method successfully allows to estimate E^* and w using only *compres-*
 275 *sive* part of the load-displacement data, thus using only *stable measurements*
 276 (Borodich et al., 2012a,b).

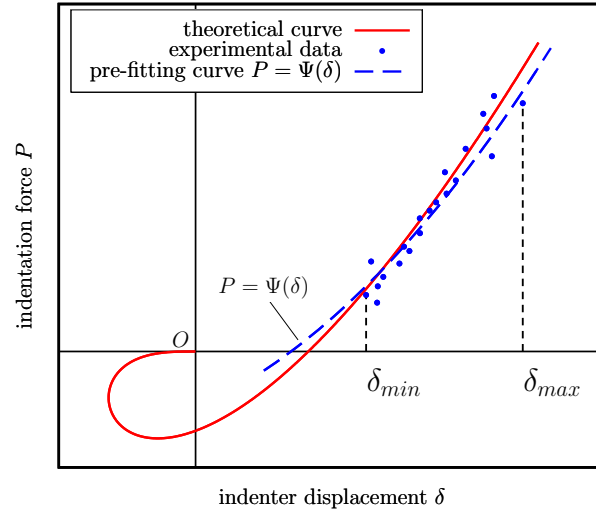
277 In the present paper, however, we use a variant of the extended BG
 278 method. This approach is particularly useful for the cases when the theoret-
 279 ical load-displacement curve is represented as a parametric function.

280 In this approach we first fit the experimental data with an auxiliary curve
 281 $P = \Psi(\delta)$ with low number of degrees of freedom. The curve acts as a high-
 282 pass filter, smoothing the data significantly (see Fig. 1,a). In the current

283 work this smoothing curve was chosen to be a polygonal chain with relatively
 284 small number of segments N_S .



(a)



(b)

Figure 1: The concept of two-stage fitting the experimental data: (a) smoothing experimental data using a polygonal chain (the preliminary fitting with an auxiliary curve), (b) fitting the theoretical load-displacement curve to the auxiliary one.

285 The point of doing so is that the auxiliary curve is supposed to have very

286 simple mathematical representation. Therefore, some advanced fitting meth-
 287 ods can be used to construct it. In this work the smoothing dimensionless
 288 curve is built as the result of minimization of the sum of squares of orthogonal
 289 distances from it to the data points (the so-called orthogonal distance fitting
 290 concept, ODF (Ahn, 2004; Boggs et al., 1987)). This approach is useful when
 291 both abscissas and ordinates of the data points are subject to measurement
 292 errors. Since the distance from a point to a straight line can be presented
 293 as a well-known formula, it is possible to *explicitly* program a function eval-
 294 uating the sum of squared orthoghonal distances and made it the subject of
 295 minimization process. Due to simple mathematical form (piece-wise linear),
 296 fitting with polygonal chain is performed extremely quickly using well-known
 297 computer algebra systems (e.g. Matlab).

298 It is important to note that the term "distance" cannot be directly applied
 299 to the space of variables of different physical meaning and of different orders
 300 of magnitude. That is the reason why the preliminary orthogonal distance
 301 fitting is performed using the normalized data:

$$\begin{aligned}\overline{\delta_n} &= \frac{\delta_n - \langle \delta_i \rangle}{\max(\delta_i) - \min(\delta_i)}, \\ \overline{P_n} &= \frac{P_n - \langle P_i \rangle}{\max(P_i) - \min(P_i)}, \\ i, n &= 1, \dots, N.\end{aligned}\tag{12}$$

where $\langle \cdot \rangle$ is the following averaging operator

$$\langle x_i \rangle = \frac{1}{N} \sum_{i=1}^N x_i.$$

302 This kind of normalization transforms all dimensionless values of force $\overline{P_n}$ and
 303 displacement $\overline{\delta_n}$ into the interval $[-1, 1]$. When the coordinates of optimal
 304 polygonal chain are found in the space of the dimensionless quantities, they
 305 can be easily recalculated back to the space of dimensional quantities by
 306 inverting the formulae (12).

307 The particular way of construction of the pre-fitting polygonal chain was
 308 chosen as follows. The polygonal chain is supposed to have N_S segments and
 309 $N_S + 1$ vertices. The first vertex is located at δ_{min} , the last one is located at

310 δ_{max} (see Fig. 1,b for reference). The abscissas of the vertices are uniformly
 311 spaced: the k -th vertex abscissa is $\delta_{Vk} = \delta_{min} + (\delta_{max} - \delta_{min})(k - 1)/N_S$.
 312 The ordinates of the vertices P_{Vk} are subject to optimal fitting the polygonal
 313 chain to the data by means of the ODF fitting in the space of dimensionless
 314 quantities (12).

315 On the second step of the extended BG method the theoretical curve (10)
 316 is fitted to the auxiliary one via adjusting P_c and δ_c . We require minimiza-
 317 tion of the squared norm of the difference between the two functions on the
 318 interval $[\delta_{min}, \delta_{max}]$ where $\delta_{min} = \min(\delta_i)$, $\delta_{max} = \max(\delta_i)$, $i = 1, \dots, N$
 319 (Fig. 1,b):

$$\Phi(P_c, \delta_c) = \int_{\delta_{min}}^{\delta_{max}} [P(\delta) - \Psi(\delta)]^2 d\delta \rightarrow \min. \quad (13)$$

320 Here $P = P(\delta)$ is the theoretical load-displacement curve, and $P = \Psi(\delta)$ is
 321 the auxiliary one.

322 Since the stable branch of (10) cannot be written as $P = P(\delta)$, we
 323 transform (13) as follows. Firstly, a dimensionless parameter \bar{a} along the
 324 theoretical curve is introduced as $P = P_c \bar{a}$. Secondly, the stable branch of
 325 the theoretical JKR curve (10) is rewritten in parametric form as

$$\begin{cases} \delta = \delta_c \left(3\sqrt{1 + \bar{a}} - 1 \right) \left(\frac{1 + \sqrt{1 + \bar{a}}}{9} \right)^{\frac{1}{3}}, \\ P = P_c \bar{a} \end{cases}, \quad (14)$$

326 OR

$$\begin{cases} \delta = \delta_c f(\bar{a}), \\ P = P_c \bar{a}. \end{cases} \quad (15)$$

327 Substitution of (15) into (13) yields:

$$\Phi(P_c, \delta_c) = \delta_c \int_{\bar{a}_{min}}^{\bar{a}_{max}} [P_c \bar{a} - \Psi(\delta_c f(\bar{a}))]^2 \frac{df}{d\bar{a}} d\bar{a} \rightarrow \min. \quad (16)$$

328 The problem (16) is the particular one used in the present study to calcu-
 329 late the optimal values of P_c and δ_c . It was done for every separate measure-

ment (data set) and the corresponding values of E^* and w were calculated using (3).

In the general case of parametrically-represented load-displacement curve

$$\begin{cases} \delta = \delta_c f_1(\bar{a}, \delta_c, P_c), \\ P = P_c f_2(\bar{a}, \delta_c, P_c), \end{cases} \quad (17)$$

the optimization problem (16) becomes

$$\Phi(P_c, \delta_c) = \delta_c \int_{\bar{a}_{min}}^{\bar{a}_{max}} [P_c f_2(\dots) - \Psi(\delta_c f_1(\dots))]^2 \frac{\partial f_1(\dots)}{\partial \bar{a}} d\bar{a} \rightarrow \min \quad (18)$$

where (\dots) denotes (\bar{a}, δ_c, P_c) .

Remark. The actual distance from the probe surface to the specimen surface is unknown. The moment when the indenter jumps into contact due to adhesion forces during loading is rather unclear due to measurement noise. This means that the origin of the δ axis is in fact unknown. Therefore, in the light of the above the measured values of δ are supposed to have an unknown additional shift value δ_s (separate for each of the DSI data sets) introduced into the readings. This value is determined as follows. A series of possible shift values is generated. Each such value is subtracted from the measured set δ_i ($i = 1, \dots, N$) and then minimization of (16) is performed. The correct shift value is supposed to give the absolute minimum of the functional values among all trial minimizations. The corresponding values of P_c and δ_c are considered to be the true ones.

3. Determination of material propertieess from a DSI experiment by the extended BG method

Let us describe a DSI-based experiment that was carried out in order to test the robustness of the modified BG method using real experimental data.

3.1. The experimental set-up and raw data pre-processing. Assumptions validation

The custom made force measurement device Basalt-1 (TETRA GmbH, Ilmenau, Germany) was used for DSI experiments (Fig. 2). In this set-up, the PVS specimen was loaded by a spherical indenter (a glass lens of known

radius $R = 5.155$ mm) attached at the end of a planar cantilever spring with constant $c = 1023.9$ N/m. The displacement of the other end of the spring was set using a piezo drive. Two fiber optical sensors S_1 and S_2 were used to control the deflections of both ends of the spring. The readings from the sensor S_2 went to the output file as total displacement δ_0 while the difference in the readings of S_1 and S_2 was recalculated into the values of applied force (in device-dependent arbitrary units) which also went to the output file. The latter values were converted to Newtons using the results of calibration.

To obtain the load-displacement dependency of the indenter, one needs to subtract the deformation of the spring from the total recorded displacement applied to the system "spring-indenter-specimen". It was done using the following formula

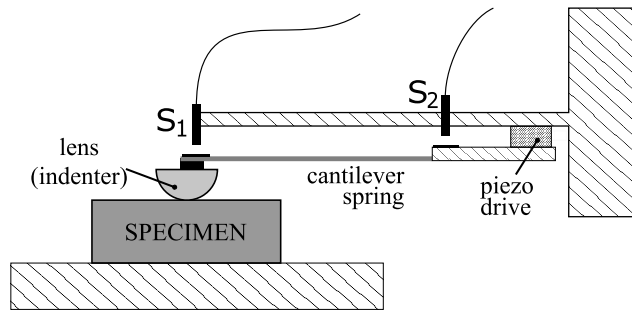
$$\delta = \delta_0 - \frac{P}{c} \quad (19)$$

where δ_0 is the total displacement applied via piezoelement, δ is the displacement of the indenter (the true displacement), P is the applied force, c is the spring stiffness.

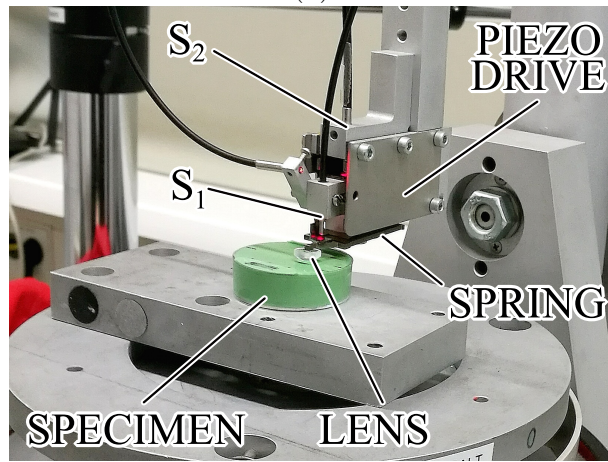
Since some measurements exhibited drift of zero point in the force value, the values of force were manually corrected for each measurement by means of a custom Matlab script. The same script was used to subtract the deformation of the spring which was done using the modified formula (19):

$$\delta = \delta_0 - \frac{P - P_{corr}}{c}$$

where P_{corr} is zero drift value. The typical processed readings are represented in Fig. 3.



(a)



(b)

Figure 2: The DSI setup: (a) the schematic, (b) the photographic image.

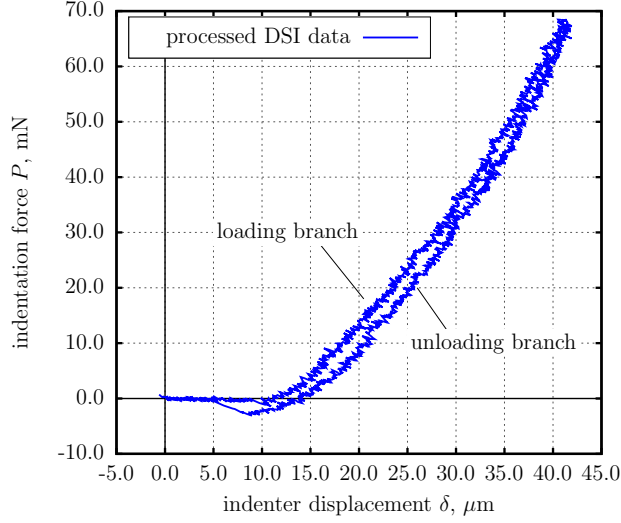


Figure 3: Typical processed DSI data (spring deflection subtracted, force readings rescaled to Newtons)

377 The specimen for DSI study consisted of a 35(diameter) x 10(height) mm
 378 Petri dish filled with two-component AFFINIS (R) light body PVS (Coltene,
 379 Switzerland) (Fig. 4,a). After filling the dish the PVS surface was covered
 380 with a clean piece of glass slide (Carl Roth, Karlsruhe, Germany) until the
 381 PVS polymerized in order to produce flat clean surface. Since PVS tends to
 382 form bubbles during moulding process, the top surface of the specimen was
 383 visually examined using optical microscope and 5 indentation locations were
 384 selected far from any visible inhomogeneity. Schematically the specimen is
 385 represented in Fig. 4,b, numbers denote measurement locations. Five DSI
 386 measurement were performed at each location which resulted in 25 data
 387 sets in total. Maximum indentation depth did not exceed 40 μm in each
 388 single experiment. The specimen was tested after approximately 16 h after
 389 polymerization.

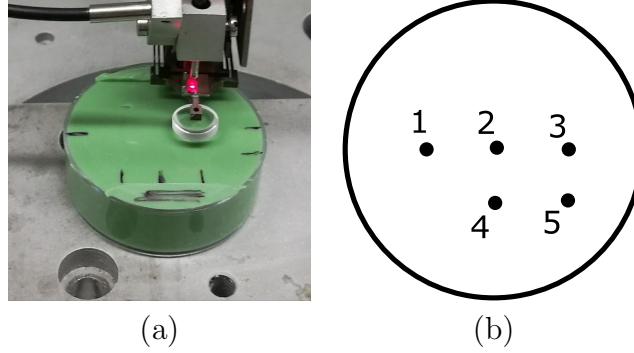


Figure 4: The PVS specimen for DSI experiment: (a) the photographic image, (b) the schematic image. Numbers denote locations of individual DSI experiments.

390 In the present work we model interaction between the indenter and the
 391 specimen as indentation of an elastic half-space. Indeed, many authors
 392 modelled indentation of finite-size specimens by means of the finite element
 393 method (FEM) (see e.g. Sadeghipour et al. (1994)). These studies show that
 394 a large enough finite specimen acts effectively as an elastic half-space. To con-
 395 firm this for the particular geometry of our specimen we use FEM in applica-
 396 tion to the problem of non-adhesive indentation of the finite volume cylindri-
 397 cal specimen of radius r and height h by a rigid sphere (see the model in Fig.
 398 5,a) The modeling was performed by means of ANSYS 18 Mechanical APDL
 399 software (<https://www.ansys.com/products/structures/ansys-mechanical-pro>)
 400 in axisymmetric formulation using the following finite element types: PLANE183
 401 for PVS; CONTA175 and TARGE169 for contact pair (the description of
 402 these element types can be found in the ANSYS software manual or in in the
 403 SNARCNET academic network [https://www.sharcnet.ca/Software/Ansys/17.2/en-](https://www.sharcnet.ca/Software/Ansys/17.2/en-us/help/ans_elem/Hlp_E_ElemTOC.html)
 404 [us/help/ans_elem/Hlp_E_ElemTOC.html](https://www.sharcnet.ca/Software/Ansys/17.2/en-us/help/ans_elem/Hlp_E_ElemTOC.html)). The indenter was assumed to be
 405 rigid, the PVS bulk was assumed to have the following properties: $E = 2.97$
 406 MPa, $\nu = 0.418$. Indentation depth was supposed to be $\delta = 40\mu\text{m}$. The
 407 obtained numerically load-displacement curves for different sizes of the spec-
 408 imen are shown in Fig. 5,b. The reference curve obtained from Hertz contact
 409 theory for a rigid sphere and an elastic half-space is shown as well (thick solid
 410 line).

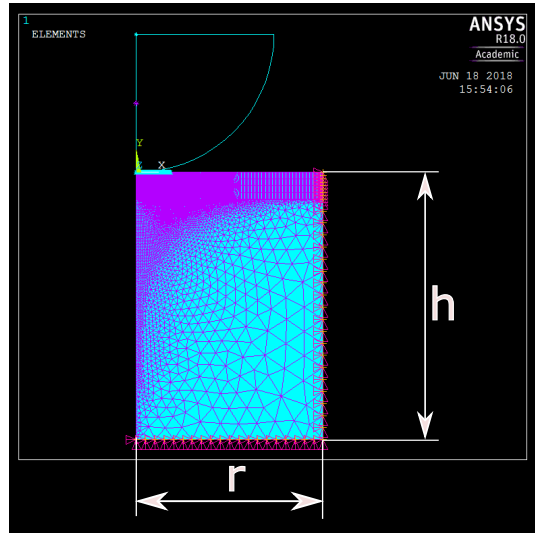
411 In these results the dashed line corresponds to measurement point No.2 on
 412 the specimen ($r=17$ mm, $h=10$ mm), while the thin solid line represents the
 413 case which is *worse* than any of the points No. 1,3,4 and 5 ($r=7$ mm, $h=10$
 414 mm). Comparison the latter two simulations at the maximum indentation

415 depth and the Hertzian model give the relative error in force value of 4.6%
416 and 6.6% correspondingly. Since FEM also introduces some inaccuracy in
417 comparison to the analytical Hertzian curve, the above results are compared
418 with the results of FEM simulation of a very large specimen ($r=68$ mm,
419 $h=40$ mm, dots in Fig. 5) which gives the relative error of 3.9% and 5.8%,
420 correspondingly.

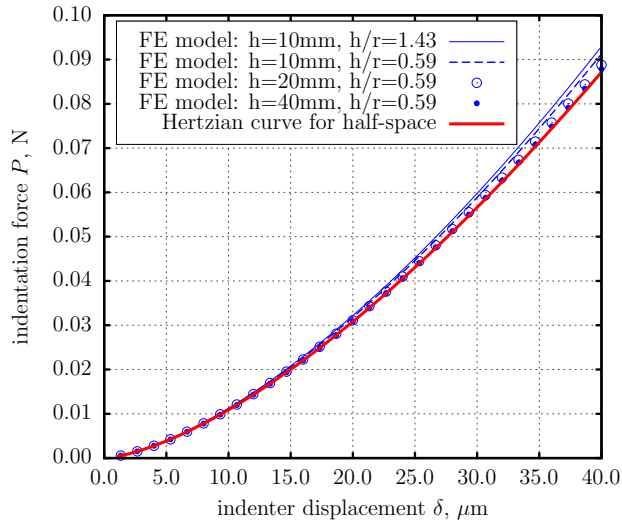
421 Thus, modeling the actual specimen as an infinite elastic half-space pro-
422 vides acceptable level of accuracy. Therefore, the mathematical apparatus of
423 the JKR theory of adhesive contact can be applied here.

424 Based on the above justification, the BG method was applied to the
425 unloading parts of the $P-\delta$ curves using the classic JKR contact theory as the
426 framework for the problem. The theoretical load-displacement dependency
427 was supposed to have the form (10) and the BG method was used in the
428 extended formulation (16).

429 The results of application of the BG method to the obtained experimental
430 data are described below.



(a)



(b)

Figure 5: Numerical modelling of indentation of a finite size specimen : (a) FEM model (axisymmetric, the right part of the axial cross-section is shown), (b) comparison of load-displacement curves obtained for different r and h : thick solid line (red) is the reference Hertzian curve for half-space; thin solid line (blue) corresponds to $h=10$ mm ($h/r = 1.43$); dashed line to $h=10$ mm ($h/r = 0.59$); circles to $h=20$ mm ($h/r = 0.59$); and dots to $h=40$ mm ($h/r = 0.59$).

3.2. The results of the DSI experiment

As it is mentioned above, 25 data sets representing unloading branches of the DSI curves were obtained in the experiment. Each of these data sets was pre-fitted with a polygonal chain. These lines were used as the pre-fitting function $P = \Psi(\delta)$ in (16). Since the number of segments in the pre-fitting polygonal chain has some influence on the identified values of E^* and w , the number of segments was varied from 4 to 10. Every time the values of E^* and w were identified separately for each of the 25 data sets. Then the averaged values $\langle E^* \rangle$ and $\langle w \rangle$ as well as the standard deviations σ_{E^*} and σ_w were computed.

As an example, in Fig. 6 the results of identification are shown for pre-fitting with 7-segment line. The complete result set is shown in the Appendix in Fig. A.19-A.21. It can be seen that the points on the (w, E^*) plane obtained using the modified BG method build very compact groups which shows that the approach (16) is robust against the measurement noise and fluctuations in data.

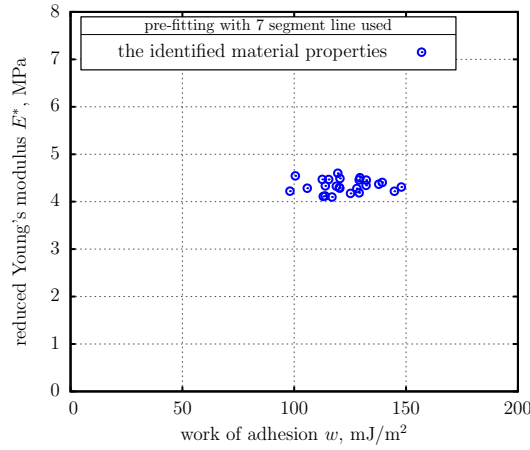
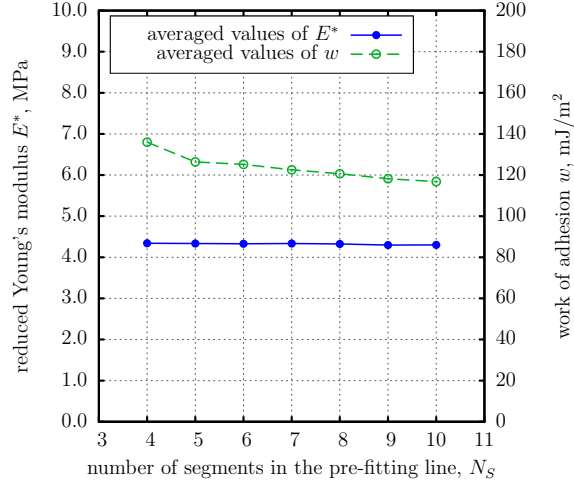


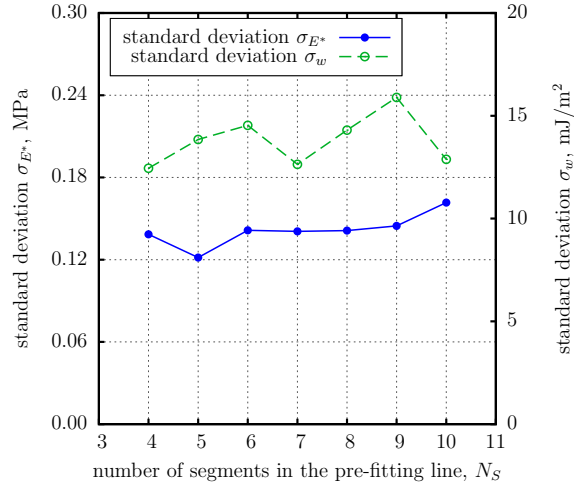
Figure 6: An example of a set of identified values of material properties extracted using pre-fitting with polygonal chain. Number of segments in chain: 7.

The dependency of the averaged values of the reduced elastic contact modulus and the work of adhesion on the number of segments is shown in Fig. 7,a. According to the presented results the averaged values of E^* vary from 4.2959 to 4.3419 MPa, the averaged values of w vary from 0.116 to 0.136 J/m². Clearly, these values do not vary much which shows that the proposed method is stable and robust with respect to chosen number of segments N_S .

453 The dependency of the values of standard deviation of the reduced elastic
 454 contact modulus and the work of adhesion on the number of segments is
 455 shown in Fig. 7,b.



(a)



(b)

Figure 7: The experimental results: (a) identified averaged PVS properties values versus the number of segments in the pre-fitting curve (the reduced elastic contact modulus and the work of adhesion), (b) standard deviations of the identified PVS properties values versus the number of segments in the pre-fitting curve.

4. The tensile experiment

The purpose of the tensile test was to validate accuracy of the BG method by evaluation of the reduced elastic contact modulus E^* of the very same PVS material using a completely different experiment, namely a standard tensile test. Since the BG method provided us with the estimated values of the *reduced* elastic modulus, one needs to evaluate both the elastic modulus and Poisson's ratio from the results of tensile testing, in order to be able to compare the results of these two experiments.

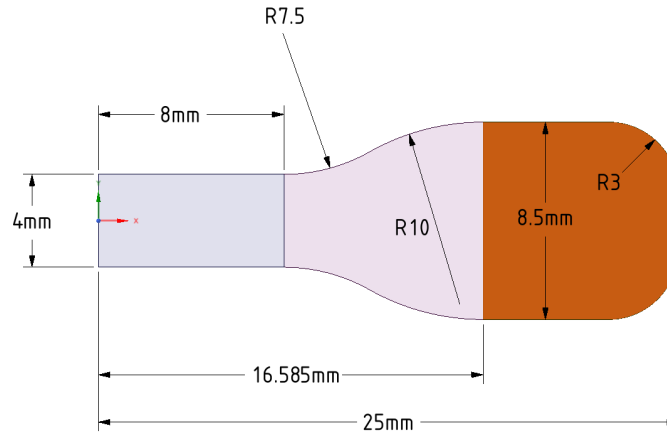
Hence, this Section consists of two independent parts. In the first part we describe the experimental evaluation of the elastic modulus of the PVS, while the second part is devoted to description of the process of estimation of the Poisson's ratio of the same material using methods of photogrammetry.

4.1. Experimental set-up and the measurements

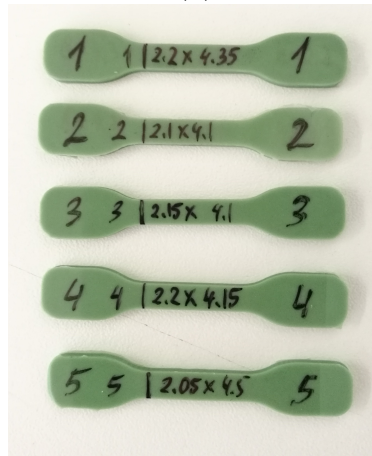
The conventional tensile testing of dumbbell specimens was carried out as an alternative way to determine the properties of PVS (Davis, 2004). The specimens were manufactured as close as possible to the requirements of ISO 37 type 3 specifications and made of exactly the same PVS charge which was used in the DSI testing. The Zwick Roell zwickiLine tensile machine and testXpert II software were employed. A schematic of the specimen is shown in Fig. 8,a. The brown shaded area corresponds to the part of the specimen being gripped by the tensile equipment. Nominal specimen thickness is 2 mm. The five actual specimens had the following dimensions of the cross-sections of the gage sections (thin parts) (thickness x width): 1) 2.2 x 4.35 mm, 2) 2.1 x 4.1 mm, 3) 2.15 x 4.1 mm, 4) 2.2 x 4.15 mm 5) 2.05 x 4.5 mm. The photographic image of the specimens is shown in Fig. 8,b. The specimens were tested approximately 18 h after moulding.

The testing was performed up to 3% of overall grip-to-grip elongation. Each specimen was tested 10 times. The recorded strain-stress curves showed that the specimens 1,3,5 produced very similar results while the two other specimens (2, 4) did not (the two lower sets of lines in Fig. 9,a). These two specimens were considered to have internal defects (most likely these defects were air bubbles inside the material) and were excluded from the further data analysis.

The tests showed that the material behavior may be well described as linearly elastic up to few percent deformation.



(a)



(b)

Figure 8: ISO37 type 3 specimens: (a) the schematic, (b) the actual specimens tested.

491 The specimens stretching during tensile test was recorded using a HD
 492 camera for evaluation of the Poisson's ratio. The methods of photogrammetry
 493 were applied to the captured images of the specimens.

494 The photographic image of the whole set-up is shown in Fig. 9,b.

495 4.2. Evaluation of elastic modulus. Correction factors for the compliance of 496 the specimens.

497 Normally, in the tensile experiment the deformation of the thin part (gage
 498 section) of the specimen is measured. This allows one to evaluate the elastic

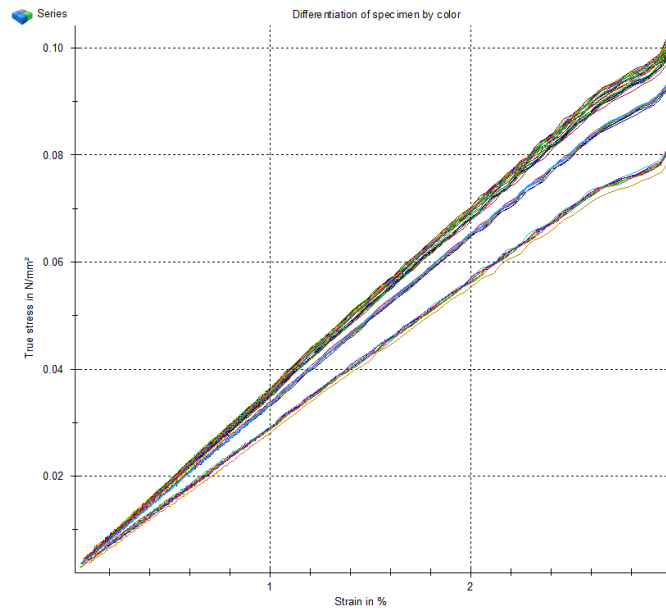
499 modulus using simplest theory of a rod under uniaxial tension.

500 Indeed, consider a rod of length L_0 and constant rectangular cross-section
501 of area $A = b_0 \cdot h$ where b_0 is its width and h is the thickness, under tensile
502 load P . Assuming homogeneous uniaxial stress condition inside the rod, the
503 elastic modulus of the material can be determined as

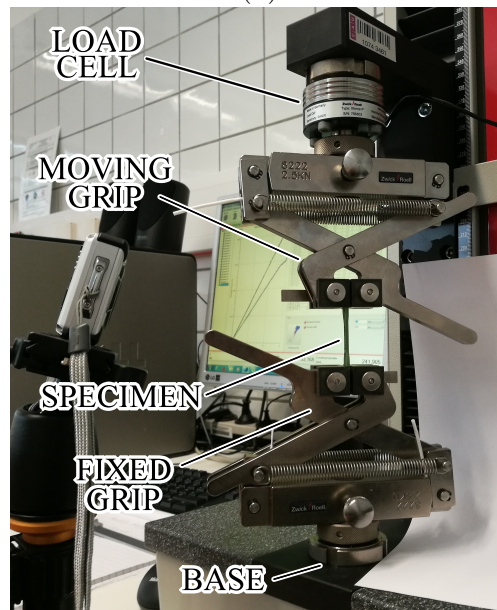
$$E = \frac{d\sigma}{d\varepsilon} = \frac{d\left(\frac{P}{A}\right)}{d\left(\frac{\Delta L_0}{L_0}\right)} = \frac{L_0}{A} \frac{dP}{d\Delta L_0} = \frac{L_0}{b_0 h} \frac{dP}{d\Delta L_0} \quad (20)$$

504 where ΔL_0 is the elongation of the rod. Assuming linear behaviour of the
505 material, one can also write

$$E = \frac{L_0}{b_0 h} \frac{P}{\Delta L_0}. \quad (21)$$



(a)



(b)

Figure 9: (a) the stress-strain curves for specimens 1-5 (screenshot of the testXpert software), (b) the experimental set-up for the tensile experiment.

506 Because our experimental set-up was not equipped with an extensometer
507 to control the deformation of the gage section of the specimens, the defor-
508 mation of the whole specimen was controlled (the grip-to-grip elongation).
509 If the grip-to-grip distance is denoted as L and the grip-to-grip elongation is
510 denoted as ΔL , then simple substitution L as L_0 and elongation of the whole
511 specimen ΔL as ΔL_0 into (21) clearly introduces some amount of inaccuracy
512 because the grip-to-grip elongation is influenced by the compliance of the
513 non-gage parts of the specimen and the machine compliance as well.

514 It should be noted that many authors argue that shape of specimens and
515 the compliance of the load cell of the tensile machine can influence the results
516 significantly. For example, Jia and Kagan (1999) provide evidences that the
517 results may differ drastically from the expected ones due to the compliance
518 of the dumbbell parts of the specimens and machine compliance. Further,
519 Sergueeva et al. (2009) found that the calculated values of elastic modulus
520 depended on the specimen geometry, in particular, on the gage length of the
521 specimen. Thus, because the specimens were made of rather soft material,
522 the influence of the compliance of the dumbbell parts of the specimens must
523 be assessed and the method for computation of the results corrected.

524 Load-cell compliance was taken into account during the factory calibra-
525 tion of the Zwick/Roell material testing machine. Therefore, this factor was
526 not considered, only the compliance of the specimen has to be analyzed.

527 Consider a dumbbell specimen of the length L and constant thickness h
528 which is subjected to tensile load by the force P . The width of the cross-
529 section is the function of the picked location $b(x)$. Let us consider the gage
530 section of the specimen subjected to uniaxial stress. This part has length
531 L_0 and cross-section width b_0 (Fig. 10). In our experiment the grip-to-grip
532 distance was $L = 33.16\text{mm}$ and the gage length was $L_0 = 10\text{mm}$ for ISO37
533 type 3 specimens. Let us follow the ideas expressed in Jia and Kagan (1999)
534 for estimation of the error introduced into the evaluated value of E when one
535 substitutes L as L_0 and elongation of the whole specimen ΔL as ΔL_0 into
536 (21).

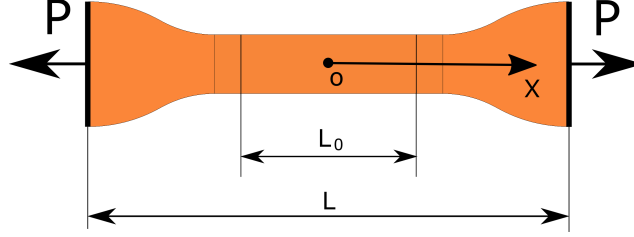


Figure 10: A dumbbell specimen under tension.

Let us denote here by E the true value of elastic modulus and by E_a the *apparent* elastic modulus, where

$$E = \frac{L_0}{b_0 h} \frac{P}{\Delta L_0}, \quad E_a = \frac{L}{b_0 h} \frac{P}{\Delta L}. \quad (22)$$

Consider the value of ΔL in (22) under the hypothesis of uniform stress across the section of the specimen

$$\begin{aligned} \Delta L(P) &= 2 \int_0^{L/2} \varepsilon(x) dx = 2 \int_0^{L/2} \frac{\sigma(x)}{E} dx = \\ &= 2 \int_0^{L/2} \frac{P}{A(x) E} dx = 2 \int_0^{L/2} \frac{P}{E h b(x)} dx = \\ &= \frac{2P}{E h} \int_0^{L/2} \frac{dx}{b(x)}. \end{aligned} \quad (23)$$

Substitution of (23) into (22) yields

$$E_a = \frac{L}{b_0 h} \frac{P}{\Delta L} = \frac{LP}{b_0 h \frac{2P}{E h} \int_0^{L/2} \frac{dx}{b(x)}} = \frac{LE}{2b_0 \int_0^{L/2} \frac{dx}{b(x)}}. \quad (24)$$

The latter gives the value of the correction factor k which is the ratio of apparent to the real elastic moduli:

$$k = \frac{E_a}{E} = \frac{L}{2b_0 \int_0^{L/2} \frac{dx}{b(x)}}. \quad (25)$$

544 Using the standard dimensions of the ISO37 specimens, the cross-section
 545 width $b(x)$ can be expressed (in millimeters) as the following piece-wise func-
 546 tion

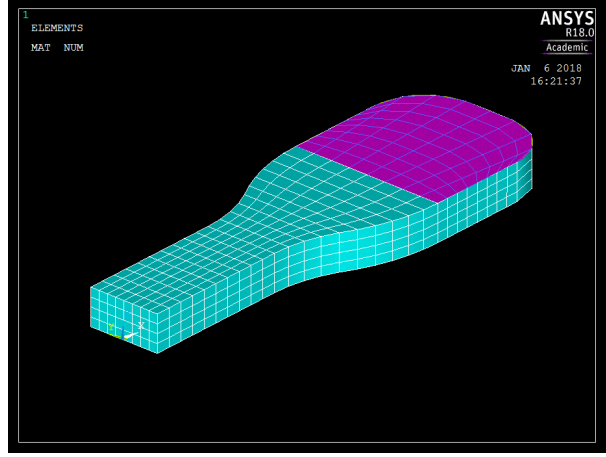
$$b(x) = 2 \begin{cases} 2 & \text{for } x \in [0; 8), \\ 9.5 - \sqrt{7.5^2 - (x - 8)^2} & \text{for } x \in [8; 11.679), \\ -5.75 + \sqrt{10^2 - (x - 16.585)^2} & \text{for } x \in [11.679; 16.585), \\ 4.25 & \text{for } x \geq 16.585. \end{cases} \quad (26)$$

547 Substitution of this function into (25) gives the value of correction factor as
 548 $k = 1.2002$. One can see that according to this rough analytical model, the
 549 real elastic modulus may be 20% lower than the apparent one which is rather
 550 a significant correction. Therefore, more thorough study is performed below.

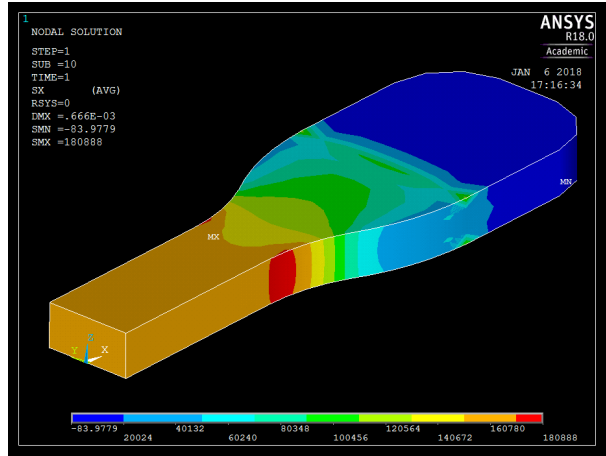
551 In order to obtain more accurate value of the correction factor k , finite
 552 element modeling of the tensile experiment was performed using ANSYS 18
 553 Mechanical APDL software in symmetric formulation (particularly, only the
 554 half of the model was built) using the SOLID186 finite element type. The
 555 FE model is depicted in Fig. 11,a. The shaded areas were the subject to
 556 nodal constraint loading: the nodal displacements UY and UZ were assigned
 557 zero values while the nodal displacements UX were assigned the value $UX =$
 558 $\Delta L/2 = 0.03L/2 = 1.33$ mm which is 1.5% of initial grip-to-grip distance. As
 559 it was mentioned earlier, the real testing was performed up to the elongation
 560 of 3% of the grip-to-grip distance.

561 Analysis of the stress distribution (Fig. 11,b) shows that this model
 562 is more accurate than the previous one since the stress distribution across
 563 the cross-section is homogeneous only in the central part of the specimen
 564 while the previous analytical model (23) model assumed this across the whole
 565 specimen.

566 Since the stress distribution in the middle part of the specimen can be
 567 considered uniaxial, the total applied force was evaluated as $P = \sigma_{x0} \cdot h \cdot b_0$,
 568 where σ_{x0} is the stress in the center of symmetry of the whole FE-modeled
 569 specimen (point O in Fig. 10).



(a)



(b)

Figure 11: FE modeling of the tensile experiment: (a) the FE model, (b) the distribution of the σ_x stresses in the specimen.

570 Since ANSYS applies loads gradually via several sub-steps, it was possible
 571 to evaluate the apparent elastic modulus using differential formula as

$$E_a = \frac{L}{b_0 h} \frac{dP}{d\Delta L}. \quad (27)$$

572 Differential formula allowed us to track changes in E_a with respect to model
 573 deformation (if any). Differentiation was performed numerically by means of
 574 ANSYS itself. Since the "true" value of E was set in the beginning of the
 575 simulation, the correction factor was computed as $k = E_a/E$.

Multiple trial runs under different parameter values showed that in linear formulation the coefficient k : (i) does not depend on the values of E in the wide range of applied stresses (1-6 MPa), (ii) slightly depends on Poisson's ratio (for a large interval of the ratio values $\nu = 0.2...0.49$, it may change approximately by 0.017), (iii) depends on specimen geometry and, in particular, for the standard ISO37 type 3 specimen made of a material with $\nu = 0.417$ it is equal to $k = 1.16977$, (iv) does not depend on specimen deformation in linear FE formulation.

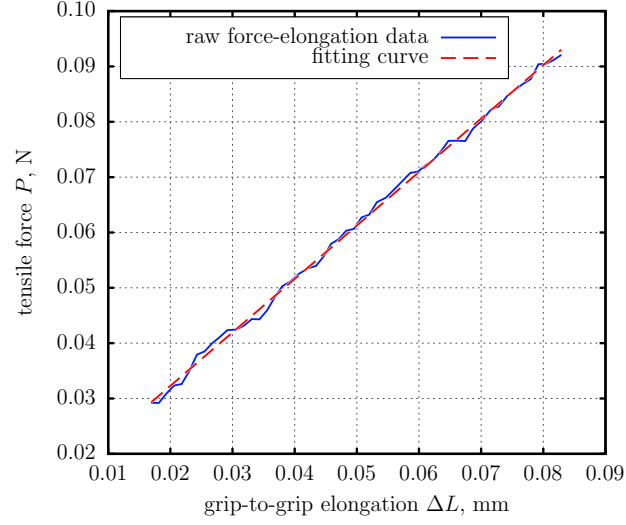
Individual values of the correction coefficients k obtained by means of ANSYS for the specimens No. 1, 3 and 5 were the following: $k_1 = 1.15294$, $k_3 = 1.16338$, $k_5 = 1.14864$.

The latter coefficients allowed us to evaluate the values of E from experimental data using the following strategy. First, for each of the three specimens and each of 10 tests per specimen, the force-elongation dependency was fitted with straight line in the interval $\frac{\Delta L}{L} \in [0.0005; 0.0025]$ and the value $\frac{dP}{d\Delta L}$ was found. Note that fitting by means of linear regression was needed because the data was rather noisy when deformations were very small (Fig. 12,a).

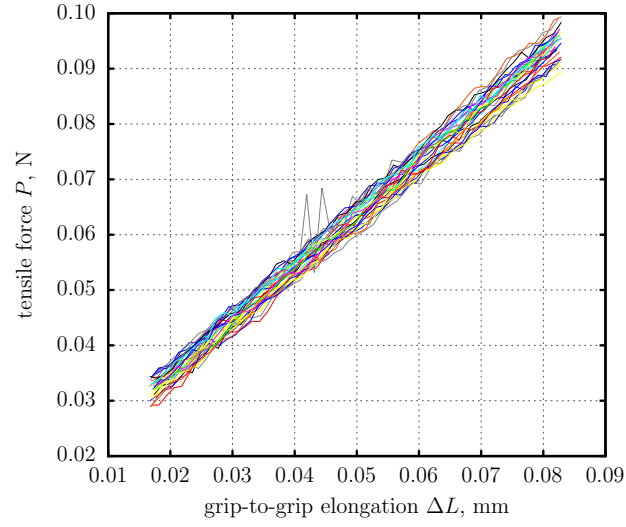
Then the apparent value of elastic modulus was evaluated using (27). The true values of E were calculated as $E = \frac{E_a}{k}$ using individual correction coefficients. Finally, the whole 30 values of E were statistically post-processed.

The raw force-elongation dependencies obtained during the experiment in the interval $\frac{\Delta L}{L} \in [0.0005; 0.0025]$ are shown in Fig. 12,b.

The computed values of the elastic modulus versus the test number for all the three specimens are presented in Fig. 13. The averaged value across all 30 data sets is $\langle E \rangle = 2.9723$ MPa. Standard deviation of the obtained data is $7.3833e-2$ MPa.



(a)



(b)

Figure 12: Force-elongation dependencies obtained during the experiment in the interval $\frac{\Delta L}{L} \in [0.0005; 0.0025]$ (raw data): (a) fitting the raw data with a straight line, (b) the raw force-elongation data for all 3 valid specimens (10 measurements per specimen).

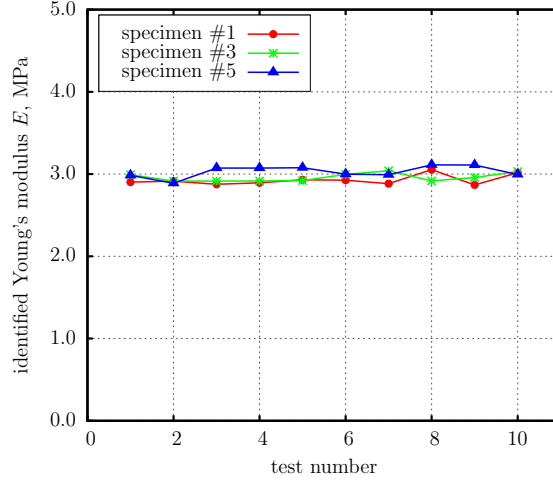


Figure 13: The computed values of the elastic modulus versus the test number. Dots: specimen 1, asterisks: specimen 3, triangles: specimen 5.

Obtaining the value of elastic modulus is not enough to validate the results of the DSI experiment in this study. In order to do so, evaluation of the Poisson's ratio of the PVS is required. The corresponding method is discussed below.

4.3. Estimation of Poisson's ratio

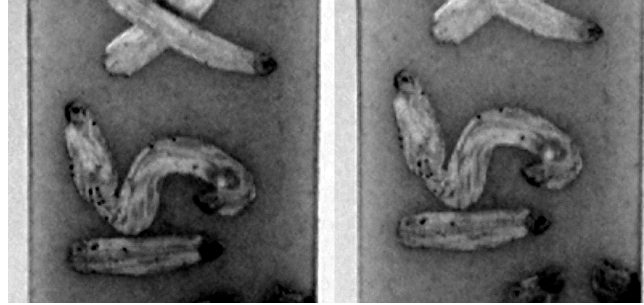
In order to estimate Poisson's ratio of the PVS, the photogrammetry approach was used that allowed us to capture the necessary data from the tensile experiments. In particular, video recording of the stretching process of the specimens was performed using a camera with HD resolution in the macro mode using different magnification factors. By extracting the photographic image of the specimen before and after stretching, it is possible to estimate the deformations in axial direction ε_x and in orthogonal direction ε_y . Poisson's ratio may be then evaluated as $\nu = -\frac{\varepsilon_y}{\varepsilon_x}$.

In the beginning all recorded videos were subject to temporal denoising and then pairs of images (before/after stretching) were extracted. These images were converted to HSV colour system and only the "Value" (V) channel was kept producing grayscale pairs of specimens' photographs. Using Matlab the contrast of these pairs of grayscale images was enhanced using the *imadjust* routine and the images were also sharpened using the *imsharpen* routine. The examples of such pairs of post-processed images are shown in

623 Fig. 14. In total, 17 image pairs of this kind were produced. Two of such
 624 image pairs are shown in the Fig. 14. In each pair, the top/left image corre-
 625 sponds to the undeformed specimen, while the bottom/right one corresponds
 626 to the stretched specimen.



(a)



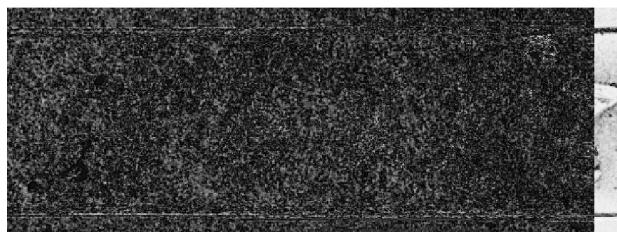
(b)

Figure 14: Examples of post-processed images used for identification of the specimens' deformations (in each pair: the top/left one is before and the bottom/right one is after stretching): (a) the images taken at low magnification, (b) images taken at high magnification.

627 Next, the Matlab routine *imregtform* was applied to each pair of images
 628 producing a global affine transform necessary to fit the image of the stretched
 629 specimen into the initial photograph of that specimen. For this purpose, in
 630 each pair one of the images was kept unchanged while the second one was
 631 deformed (including shift, shear, stretching and rotation) so that finally it
 632 became a part of the first image (or they had some parts in common). This
 633 is the so-called image registration process.

634 In order to assure the quality of performed image registration, the differ-

635 ence between the images was computed for each pair. In a pair of grayscale
636 images each one is essentially a matrix with integer values in 0..255 range.
637 Hence, the difference image is a matrix containing the absolute values of the
638 result of their subtraction. If some features in the two images coincide, the
639 dark area on the difference image is produced. Only the features that do not
640 coincide are highlighted because they have a non-zero difference in the lumi-
641 nosity values. Examples of such difference images corresponding to Fig. 14
642 are shown in Fig. 15. It can be noted that the difference images contain only
643 noise and do not contain the features of the original images which is a good
644 evidence of successful registration. That is, the affine transform allowing to
645 fit the right image into the left one was computed with high accuracy. More
646 on digital image processing methods can be found in Gonzalez and Woods
647 (2018) and the corresponding sections of Matlab manual.



(a)



(b)

Figure 15: Examples of difference images produced for image pairs after registration. There are no features of the original images in the regions where subtraction was performed which is the sign of successful registration. The brightness is increased for illustrative purpose.

648 Next, the above mentioned affine transform was inverted producing the
 649 transform from initial to stretched state. The produced affine transform
 650 contains information about translation, rotation, axial and shear deforma-
 651 tions necessary to fit one image into another. Since image registration via
 652 *imregtform* was performed iteratively as the result of Matlab's internal op-
 653 timization algorithm, the obtained transforms did not purely contain axial
 654 deformations but also small amount of the other types of transformation.
 655 In order to extract the information about axial deformations in vertical and
 656 horizontal directions it was decided to apply the obtained transform to a set
 657 of points with known coordinates initially forming a square (Fig.16,a). Let
 658 a be the side length of this square.

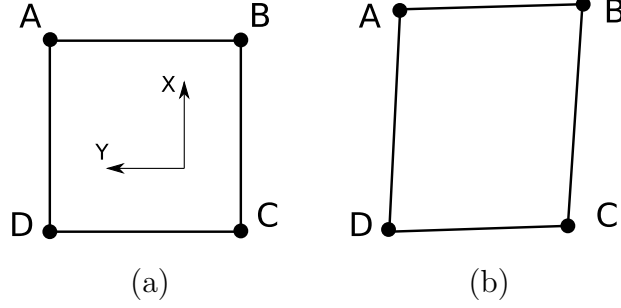


Figure 16: Set of four points forming a quadrangle before and after application of the identified affine transform: (a) initial state, (b) deformed state. The amount of shear deformation is increased for illustrative purpose.

659 After evaluation of the coordinates of the vertices of the deformed square
 660 the absolute values of axial deformations were estimated as follows

$$\begin{aligned}\varepsilon_x &= \frac{\frac{|x_A - x_D| + |x_B - x_C|}{2} - a}{a}, \\ \varepsilon_y &= \frac{\frac{|y_A - y_B| + |y_D - y_C|}{2} - a}{a}.\end{aligned}\tag{28}$$

661 Finally, Poisson's ratio was computed as

$$\nu = -\frac{\varepsilon_y}{\varepsilon_x}.\tag{29}$$

662 The results of evaluation of Poisson's ratio values for all 17 image pairs
 663 is represented in Fig. 17. The averaged value is $\nu = 0.41758$, the standard
 664 deviation is $\sigma_\nu = 0.0147$.

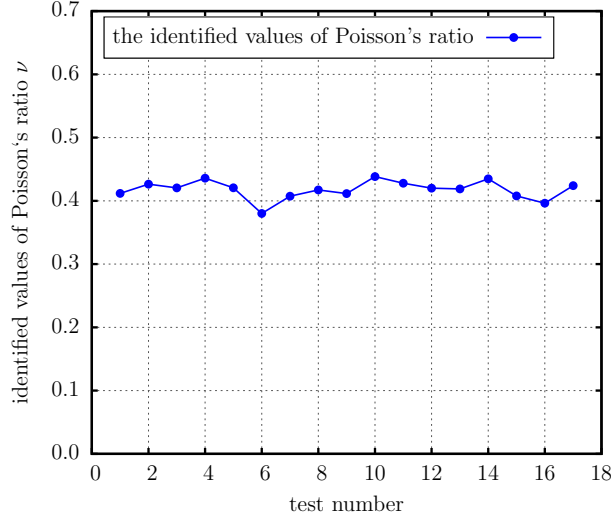


Figure 17: The computed values of the Poisson's ratio for different captured images.

5. Comparison of the results of two experiments

Now the results of the two different experiments can be compared. As it has been discussed above, the experimental results are influenced by many factors related to the used equipment, mathematical algorithms, and assumptions of different kinds. Let us analyse briefly some of these factors.

Two types of noise were present in the measured DSI data: high-frequency noise and small low-frequency fluctuations that influenced the overall trend of load-displacement curves. The noise was produced mostly from the electronic circuits of the DSI sensors and was effectively eliminated by the pre-fitting curve. Slow fluctuations in the data can be caused by small inhomogeneities of properties of the surface of the specimen. Influence of these factors was minimized by multiple repeated testing at different locations. A pre-fitting curve with the low number of degrees of freedom may also smooth away 'bumps' in the measured load-displacement sequence.

The experimental results showed in Fig. A.19-A.20 are packed in rather tight clouds of points which demonstrate the robustness and accuracy of the tested BG approach. However, the optimal number of segments in the pre-fitting polygonal chain may be the matter of discussion because the obtained results do not exhibit a clearly visible optimum, e.g. global minimum in standard deviation etc., and low number of segments leads to unreason-

685 able increase in the identified values of the work of adhesion. In any case,
686 the results corresponding to different numbers of segments in the pre-fitting
687 polygonal chain do not differ significantly.

688 In the DSI experiment we used the JKR theory of adhesive contact as the
689 theoretical background. This theory requires the tested elastic medium to be
690 a half-space. Using numerical simulations, we showed in the corresponding
691 Section that the thick PVS specimen effectively models properties of an elas-
692 tic half-space, given that indentation depth is small. However, the finite size
693 specimen is stiffer than a half-space which means that the actual measured
694 values of indentation force were slightly higher than it would be expected.
695 The same effect may also be caused by non-linearity of the constitutive law
696 for PVS. As PVS is a hyperelastic material, it means that non-linear compo-
697 nents of stresses - however small they might be - make the specimen material
698 appear stiffer during compression in comparison to purely linear case or in
699 comparison to tensile load.

700 Altogether, the above means that the values of the reduced elastic contact
701 modulus E^* obtained by means of the BG method using that particular
702 specimen are slightly higher than they could be if the BG method was applied
703 to a data obtained using a linearly elastic half-space.

704 On the other hand, the tensile experiment has its own sources of possible
705 inaccuracies. It can be seen that at small deformation range (at which elas-
706 tic modulus is usually identified) the obtained force-elongation data is rather
707 noisy (Fig. 12). This issue has been overcome by means of fitting the data
708 with straight line. Normally, the obtained values of both the force and elon-
709 gation are used in conventional formulae of the materials science describing
710 a rod under tension which allows to estimate the value of the elastic modulus
711 quite easily.

712 Clearly, it was not the case in our experiment because the elongation
713 of the gage section of the specimens could not be measured directly and
714 the deformation of the whole specimen was measured instead. Therefore, we
715 studied how the identified values of elastic modulus depend on the compliance
716 of the non-gage parts of the sample. Both analytical and numerical modeling
717 provided similar values of the correction factor k (the ratio of the apparent to
718 the real elastic moduli). Similarity of these results obtained in different ways
719 indicates that the obtained value of the correction factor is rather correct.

720 Finite element model indeed provided more accurate values of k since it
721 better reproduced stress distribution in the specimen. However, the presence
722 of grip force was not taken into account in it. It is expected that if grip

723 pressure is applied to the grip area in the FE model (shaded areas in Fig.
724 8,a and Fig. 11,a) instead of zero normal displacements, it causes reduction
725 in the tension of the gage section as material is "squeezed" out of the grip.
726 In turn, this should reduce the computed correction factors k . Thus, the
727 real identified values of the elastic modulus of the PVS are likely to be a
728 little higher than the presented in the previous Section because they were
729 calculated as $E = E_a/k$.

730 Poisson's ratio of the PVS in this work was not determined from a sep-
731 arate dedicated experiment but rather estimated using photogrammetry ap-
732 proaches. Simple determination of deformations using changes in distance
733 between features in specimens' photographs might be an unreliable approach
734 when processing images containing noise. Hence, we applied ready-to-use
735 Matlab routines for image registration which computed a global transform
736 needed to fit the photograph of the stretched specimen into the photograph
737 of the unstretched one. In this case the entire image was used as the source
738 of metric calculation for image fitting algorithm. As the result, the obtained
739 estimated values of Poisson's ratio looked pretty stable with respect to differ-
740 ent zoom factors used and different amounts of noise present in the processed
741 images. This is an implicit evidence of the correctness of the obtained results.
742 It also should be noted here that PVS is a rubber-like material. So we expect
743 that in case of any inaccuracies the real values of Poisson's ration should not
744 be less than the identified value $\nu = 0.41758$ but even higher than that. In
745 that case, the value of E^* identified in the tensile experiment should also be
746 higher.

747 Applying the extended BG method to the results of the DSI tests, the
748 values of the reduced elastic contact modulus E^* and the work of adhesion
749 w of the tested material were obtained. The averaged values of E^* varied
750 from 4.2959 to 4.3419 MPa, while the averaged values of w varied from 0.116
751 to 0.136 J/m² depending on the number of segments in the pre-fitting line.
752 Indeed, the identified values of the reduced contact modulus and the work of
753 adhesion depend on the theory of adhesive contact used as the mathematical
754 model for the indentation experiment. Hence, the use of the JKR theory as
755 the framework for the problem must be justified.

756 In their papers Tabor (1977) and Muller et al. (1980) (see also Maugis
757 (2000)) introduced a dimensionless parameter suitable for clear distinction
758 of applicability range between the JKR and the DMT theories of adhesive
759 contact:

$$\mu = \left(\frac{Rw^2}{E^{*2}z_0^3} \right)^{1/3} \quad (30)$$

where R is the effective curvature radius of contacting bodies (if a sphere is in contact with a plane, R is equal to the radius of the sphere, that is $R = 5.155$ mm); z_0 is the equilibrium distance between atoms of the contacting bodies, usually assumed to be 0.3...0.5 nm.

Values $\mu \gg 1$ indicate that the experiment is in the applicability range of the JKR theory, while values $\mu \ll 1$ suggest that the DMT theory should be used. Assuming $z_0 = 0.4$ nm and using the total maximum and minimum identified values of E^* and w among all calculations (see Table 1 and 2 below) one can estimate the range of values of the parameter μ as follows:

$$\mu_{min} = \left(\frac{Rw_{min}^2}{E_{max}^{*2}z_0^3} \right)^{1/3}$$

and

$$\mu_{max} = \left(\frac{Rw_{max}^2}{E_{min}^{*2}z_0^3} \right)^{1/3}$$

where the subscripts "max" and "min" denote the maximum and the minimum identified values of the corresponding physical quantities.

The calculated values of the Tabor-Muller parameters were: $\mu_{min} = 2930.2$, $\mu_{max} = 5014.1$. Thus, the DSI tests in the present work fall within the range of applicability of the JKR theory.

In the second experiment, tensile testing of dumbbell PVS specimens was performed. The obtained data allowed us to evaluate the values of elastic modulus and Poisson's ratio of the material of the specimens. The corresponding values were $E = 2.9723$ MPa (averaged across the set of 30 values with minimum identified value of 2.8687 MPa and maximum identified value of 3.1121 MPa) and $\nu = 0.41758$ (averaged across the set of 17 values with minimum identified value of 0.37999 and maximum identified value of 0.43827) which gave us the value of the estimate value of the reduced elastic contact modulus as $E^* = E/(1 - \nu^2) = 3.60005$ MPa. Using the above minimum and maximum values of E and ν one can find that the lowest and the highest individual identified values of the reduced elastic contact modulus E^* in the tensile experiment were 3.353 MPa and 3.852 MPa respectively.

Table 1 contains minimum, maximum, and averaged values of the reduced elastic contact modulus E^* identified by means of the BG method from the

DSI experiment (depending on the number of segments N_S in pre-fitting line). The relative differences with the tensile experiment (based on mean values) are shown as well. The relative differences Δ_{rel} in the identified values were computed as

$$\Delta_{rel} = \frac{|E_{TENS}^* - E_{DSI}^*|}{E_{DSI}^*} \quad (31)$$

where E_{TENS}^* and E_{DSI}^* are the values identified from the tensile experiment and in the DSI experiment (by means of the BG method) respectively.

Graphical comparison of the results of the two experiments (identification of E^*) is shown in Fig. 18. Filled rectangles denote total ranges of individual identified values of E^* in all calculations. Dots denote averaged values of E^* . Percentages denote relative difference in values calculated according to (31). In case of the DSI experiment the BG method was used. Hence, multiple dots correspond to different values of N_S in pre-fitting.

Detailed comparison of the values of E^* calculated in the two experiments (Fig. 18) showed that the relative difference (31) between total maximum in the tensile experiment and the total minimum in the DSI experiment was 3.80%. The relative difference between total minimum in the tensile experiment and the total maximum in the DSI experiment was 27.38%. The relative difference in averaged values of E^* varied between 16.20% and 17.09% depending on the number of segments N_S used during pre-fitting. This can be considered as a good result.

Summarizing all the above considerations, we note that due to the sample size effect and the material properties the values of E^* identified by means of the BG method were slightly higher than they could have been. At the same time, due to shortcomings in the processing of the data of the tensile experiment the identified values of E^* were lower than they could be. Thus, the difference in results of the two experiments could be even smaller than the figures of 16.20 ... 17.09% stated above. Thus, the accuracy of the extended BG method in formulation (16) has been directly confirmed.

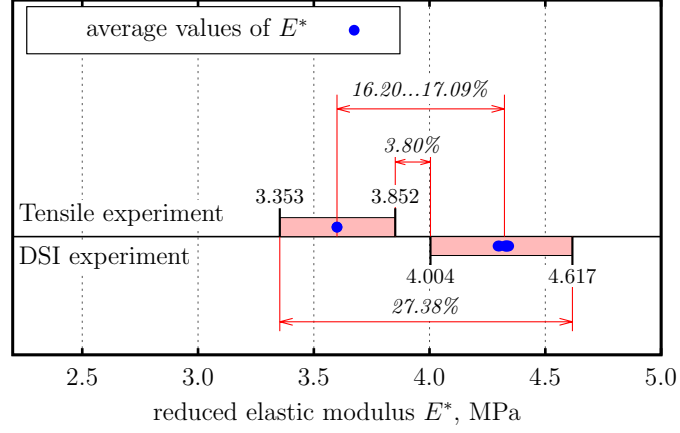


Figure 18: Graphical comparison of the results of the two experiments (identification of E^*). Filled rectangles: total ranges of individual identified values of E^* in all calculations; dots: averaged values; percentages denote relative differences (31). In case of the DSI experiment the BG method was used. Hence, multiple dots correspond to different values of N_S in pre-fitting.

Table 1: Minimum, maximum, averaged values of the reduced elastic contact modulus E^* identified by means of the BG method, and the relative difference from the results of the tensile experiment $\Delta_{rel.avg}$ for averaged values versus the number of segments N_S in pre-fitting line.

N_S	min E^* , MPa	max E^* , MPa	avg E^* , MPa	$\Delta_{rel.avg}$, %
4	4.004	4.544	4.342	17.09
5	4.131	4.558	4.336	16.97
6	4.027	4.541	4.329	16.84
7	4.099	4.599	4.334	16.93
8	4.051	4.586	4.325	16.76
9	4.065	4.609	4.296	16.20
10	4.064	4.617	4.302	16.32

Table 2: Minimum, maximum, averaged values of the work of adhesion w identified by means of the BG method versus the number of segments N_S in pre-fitting line.

N_S	min w , J/m ²	max w , J/m ²	avg w , J/m ²
4	0.1042	0.1584	0.1360
5	0.1022	0.1536	0.1264
6	0.0832	0.1468	0.1252
7	0.0981	0.1479	0.1226
8	0.0816	0.1555	0.1207
9	0.0879	0.1489	0.1182
10	0.0966	0.1476	0.1168

816 Conclusions

817 In this work a concept of a model-based approach to simultaneous identi-
818 fication of elastic (the reduced elastic contact modulus E^*) and adhesive (the
819 work of adhesion w) properties of materials and structures from experimen-
820 tal results of depth sensing indentation (DSI) has been presented. This new
821 approach is an extended version of the BG method developed by Borodich
822 and Galanov (2008) which uses different objective functional and the idea of
823 preliminary smoothing the data.

824 The extended BG method uses the concept of two-stage fitting of the
825 theoretical DSI dependency to the experimental data points. Firstly, the
826 data is fitted with an auxiliary curve which acts as a filter in certain sense.
827 The mathematical representation of this pre-fitting curve is supposed to be as
828 simple as possible. This allows us to use some advanced fitting/filtering tech-
829 niques to reduce measurement noise and fluctuations in the data. Secondly,
830 the theoretical load-displacement curve (the expected DSI dependency which
831 may be a complex expression) is fitted to the auxiliary one via minimization
832 of the squared norm of the difference of the two functions (the objective func-
833 tional). The sought material properties are determined from the optimal set
834 of characteristic parameters that give minimum to the objective functional.

835 The accuracy and robustness of the above approach has been directly
836 validated by means of two independent experiments in which the properties
837 of specimens made of polyvinyl siloxane (PVS) were determined. Both ex-
838 periments allowed us to evaluate the values of the reduced elastic modulus
839 E^* of the PVS and compare these values.

840 In the first experiment a DSI equipment was used and the BG method

841 was applied to the obtained data as described above using the JKR theory
842 of adhesive contact as the theoretical background for the problem. The
843 pre-fitting curve was chosen to be a polygonal chain. It was fitted to the
844 normalized (dimensionless) data using orthogonal distance fitting approach
845 which has advantage over conventional least-squares fitting when both force
846 and displacement readings are supposed to have measurement errors.

847 In the second experiment we performed tensile testing of dumbbell PVS
848 specimens while taking video recording of the stretching process. The ob-
849 tained data allowed us to separately evaluate the values of elastic modulus
850 and Poisson's ratio of the material of the specimens and then calculate the
851 value of the reduced elastic modulus of the material.

852 Comparison of the of the results of the two experiments showed that the
853 absolute minimum in relative difference between individual identified values
854 of the reduced elastic modulus E^* in the two experiments was 3.80%; the
855 absolute maximum of the same quantity was 27.38%; the relative difference
856 in averaged values of E^* varied between 16.20% and 17.09% depending on
857 the number of segments N_S used during pre-fitting. The above can be con-
858 sidered as a good result. Our analysis showed that unaccounted factors and
859 phenomena tend to decrease the differences in the results of the two experi-
860 ments. Therefore, the results obtained by means of the two different methods
861 in this work should differ even less.

862 However, since the results of the two experiments coincide well enough,
863 it can be concluded that the methods used in both experiments are rather
864 effective and well justified as well as the used assumptions. Thus, the ro-
865 bustness and accuracy of the proposed extension of the BG method has been
866 directly validated.

867 Acknowledgements

868 This collaborative work between Cardiff University, UK and Christian-
869 Albrechts-Universität zu Kiel, Germany was initiated as a part of activities of
870 the CARBTRIB International Network supported by the Leverhulme Trust.
871 The authors are grateful to the Leverhulme Trust for the support of their
872 collaboration.

873 The visits of Prof. Feodor Borodich and Dr. Nikolay Perepelkin to the
874 Functional Morphology and Biomechanics Group at Kiel University were sup-
875 ported by Alexander von Humboldt Foundation and the European Union's

876 Horizon 2020 research and innovation programme under the Marie Skłodowska-
877 Curie grant agreement No 663830 respectively. Thanks are due to Alexander
878 von Humboldt Foundation and the Marie Skłodowska-Curie programme.

879 References

880 Ahn, S. J., 2004. Least Squares Orthogonal Distance Fitting of Curves and
881 Surfaces in Space. Springer-Verlag, Berlin.

882 Al-Musawi, R. S., Brousseau, E. B., Geng, Y., Borodich, F. M., 2016. Insight
883 into mechanics of afm tip-based nanomachining: bending of cantilevers and
884 machined grooves. *Nanotechnology*. 27, 385302.

885 Argatov, I. I., Borodich, F. M., Epshtein, S. A., Kossovich, E. L., 2017.
886 Understanding of material properties of thin films attached to sub-
887 strates: depth-sensing unloading of elasto-plastic and elasto-brittle ma-
888 terials. *Mech. Mater.* 114, 172–179.

889 Beach, E. R., Tormoen, G. W., Drelich, J., Han, R., 2002. Pull-off force mea-
890 surements between rough surfaces by atomic force microscopy. *J. Colloid*
891 *Interface Sci.* 247 (1), 84–99.

892 Boggs, P. T., Byrd, R. H., Schnabel, R. B., 1987. A stable and efficient
893 algorithm for nonlinear orthogonal distance regression. *SIAM J. Sci. Stat.*
894 *Comput.* 8 (6), 1052–1078.

895 Borodich, F. M., 2014. The Hertz-type and adhesive contact problems for
896 depth-sensing indentation. *Adv. App. Mech.* 47, 225–366.

897 Borodich, F. M., Galanov, B. A., 2008. Non-direct estimations of adhesive
898 and elastic properties of materials by depth-sensing indentation. *Proc. R.*
899 *Soc. Ser. A.* 464, 2759–2776.

900 Borodich, F. M., Galanov, B. A., Gorb, S. N., Prostov, M. Y., Prostov,
901 Y. I., Suarez-Alvarez, M. M., 2012a. Evaluation of adhesive and elastic
902 properties of materials by depth-sensing indentation of spheres. *J. App.*
903 *Phys. A: Mater. Sci. and Processing.* 108 (1), 13–18.

904 Borodich, F. M., Galanov, B. A., Gorb, S. N., Prostov, M. Y., Prostov, Y. I.,
905 Suarez-Alvarez, M. M., 2012b. An inverse problem for adhesive contact

- 906 and non-direct evaluation of material properties for nanomechanics appli-
 907 cations. *Nanoscale Systems: Mathematical Modeling, Theory and Appli-*
 908 *cations*. 1, 80–92.
- 909 Borodich, F. M., Galanov, B. A., Gorb, S. N., Prostov, M. Y., Prostov, Y. I.,
 910 Suarez-Alvarez, M. M., 2013. Evaluation of adhesive and elastic properties
 911 of polymers by the bg method. *Macromol. React. Eng.* 7, 555–563.
- 912 Borodich, F. M., Keer, L. M., 2004a. Contact problems and depth-sensing
 913 nanoindentation for frictionless and frictional boundary conditions. *Int. J.*
 914 *Solids Struct.* 41, 2479–2499.
- 915 Borodich, F. M., Keer, L. M., 2004b. Evaluation of elastic modulus of ma-
 916 terials by adhesive (no-slip) nanoindentation. *Proc. R. Soc. Ser. A.* 460,
 917 507–514.
- 918 Boyd, S., Vandenberghe, L., 2004. *Convex Optimization*. Cambridge Univ.
 919 Press.
- 920 Bull, S. J., 2005. Nanoindentation of coatings. *J. Phys. D: App. Physics.* 38,
 921 393–413.
- 922 Bulychev, S. I., Alekhin, V. P., Shorshorov, M. K., Ternovskii, A. P., Shnyrev,
 923 G. D., 1975. Determination of young’s modulus according to indentation
 924 diagram (in Russian). *Industrial Laboratory* 41, 1409–1412.
- 925 Bulychev, S. I., Alekhin, V. P., Shorshorov, M. K., Ternovskii, A. P., Shnyrev,
 926 G. D., 1976. Mechanical properties of materials studied from kinetic dia-
 927 grams of load versus depth of impression during microimpression (in Rus-
 928 sian). *Strength of Materials.* 8, 1084–1089.
- 929 Carrillo, F., Gupta, S., Balooch, M., Marshall, S., Marshall, G., Pruitt, L.,
 930 Puttlitz, C., 2005. Nanoindentation of polydimethylsiloxane elastomers:
 931 Effect of crosslinking, work of adhesion, and fluid environment on elastic
 932 modulus. *J. Mater. Research.* 20 (10), 2820–2830.
- 933 Chai, J., Takahashi, Y., Lautenschlager, E. P., 1998. Clinically rele-
 934 vant mechanical properties of elastomeric impression materials. *Int. J.*
 935 *Prosthodont.* 11, 219–223.

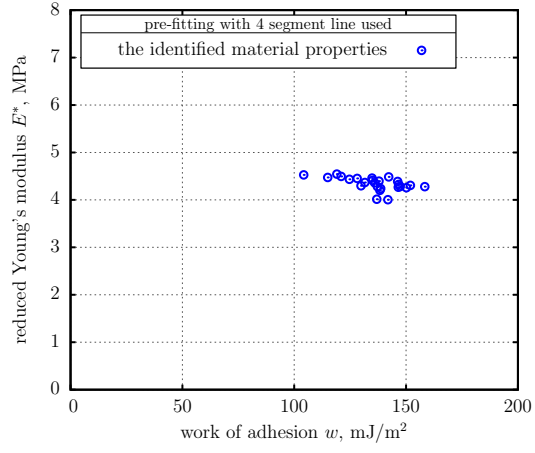
- 936 Chaudhri, M. M., Lim, Y. Y., 2007. Nanoindentation techniques: A critical
937 assessment of the current methods of data analysis. *Key Engineering*
938 *Materials*. 345-346, 1107–1114.
- 939 Chong, E., Zak, S., 2001. *An introduction to optimization*. Wiley, New York.
- 940 Davis, J. R., 2004. *Tensile Testing* (2nd Ed.). ASM International.
- 941 Derjaguin, B. V., Muller, V. M., Toporov, Y. P., 1975. Effect of contact
942 deformations on adhesion of particles. *J. Colloid Interface Sci.* 53, 314–326.
- 943 Doerner, M. F., Nix, W. D., 1986. A method for interpreting the data from
944 depth-sensing indentation instruments. *J. Mater. Research*. 1, 601–609.
- 945 Ebenstein, D. M., Wahl, K. J., 2006. A comparison of JKR-based methods
946 to analyze quasi-static and dynamic indentation force curves. *J. Colloid*
947 *Interface Sci.* 298, 652–662.
- 948 Galanov, B. A., Dub, S. N., 2017. Critical comments to the Oliver–Pharr
949 measurement technique of hardness and elastic modulus by instrumented
950 indentations and refinement of its basic relations. *J. Superhard Mater.*
951 39 (6), 373–389.
- 952 Galanov, B. A., Grigor’ev, O. N., Mil’man, Y. V., Ragozin, I. P., 1983.
953 Determination of the hardness and Young’s modulus from the depth of
954 penetration of a pyramidal indenter. *Strength of Materials*. 15, 1624–1628.
- 955 Galanov, B. A., Grigor’ev, O. N., Mil’man, Y. V., Ragozin, I. P., Trefilov,
956 V. I., 1984. Determination of the hardness and Young’s modulus with
957 elastoplastic penetration of indentors into materials. *Sov. Phys. Dokl.* 29,
958 146–147.
- 959 Gonzalez, R. C., Woods, R. E., 2018. *Digital Image Processing* (4th Ed.).
960 Pearson Education Inc.
- 961 Gorb, E. V., Gorb, S. N., 2009. *IUTAM Symposium on Scaling in Solid*
962 *Mechanics*. Springer, Dordrecht, Ch. Contact Mechanics at the Insect-
963 Plant Interface: How Do Insects Stick and How Do Plants Prevent This?,
964 pp. 243–252.

- 965 Grierson, D. S., Flater, E. E., Carpick, R. W., 2005. Accounting for the
966 JKR–DMT transition in adhesion and friction measurements with atomic
967 force microscopy. *Journal of Adhesion Science and Technology*. 19, 291–
968 311.
- 969 Jia, N., Kagan, V. A., 1999. Limitations of Test Methods
970 for Plastics, ASTM STP 1369. American Society for Test-
971 ing and Materials, West Conshohocken, PA, Ch. Interpretations of Tensile Properties of Polyamide 6 and PET Based
972 Thermoplastics Using ASTM and ISO Procedures, available at
973 <http://www8.basf.us//PLASTICSWEB/displayanyfile?id=0901a5e180004890>.
974
- 975 Johnson, K. L., 1985. *Contact Mechanics*. Cambridge University Press, Cam-
976 bridge.
- 977 Johnson, K. L., Kendall, K., Roberts, A. D., 1971. Surface energy and the
978 contact of elastic solids. *Proc. R. Soc. Lond. A*. 324, 301–313.
- 979 Kalei, G. N., 1968. Some results of microhardness test using the depth of
980 impression (in Russian). *Mashinovedenie*. 4 (3), 105–107.
- 981 Maugis, D., 2000. *Contact, Adhesion and Rupture of Elastic Solids*. Springer-
982 Verlag, Berlin.
- 983 Muller, V. M., Yushchenko, V. S., Derjaguin, B. V., 1980. On the influence
984 of molecular forces on the deformation of an elastic sphere and its sticking
985 to a rigid plane. *J. Colloid Interface Sci.* 77 (1), 91–101.
- 986 Oliver, W. C., Pharr, G. M., 1992. Improved technique for determining hard-
987 ness and elastic modulus using load and displacement sensing indentation
988 experiments. *J. Mater. Research*. 7, 1564–1580.
- 989 Popov, V. L., 2010. *Contact mechanics and friction*. Springer, Heidelberg.
- 990 Rundlöf, M., Karlsson, M., Wågberg, L., Poptoshev, E., Rutland, M., Claes-
991 son, P., 2000. Application of the JKR method to the measurement of ad-
992 hesion to Langmuir-Blodgett cellulose surfaces. *J. Colloid Interface Sci.*
993 230 (2), 441–447.
- 994 Sadeghipour, K., Chen, W., Baran, G., 1994. Spherical micro-indentation
995 process of polymer-based materials: a finite element study. *J. Phys. D:*
996 *Appl. Phys.* 27, 1300–1310.

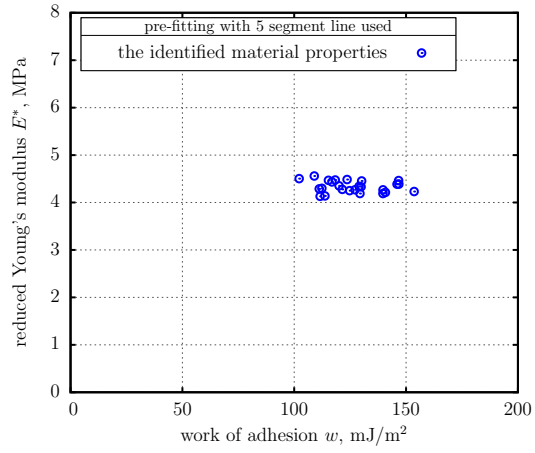
- 997 Sergueeva, A. V., Zhou, J., Meacham, B. E., Branagan, D. J., 2009. Gage
998 length and sample size effect on measured properties during tensile testing.
999 Materials Science and Engineering: A. 526 (1), 79–83.
- 1000 Shorshorov, M. K., Bulychev, S. I., Alekhin, V. P., 1981. Work of plastic
1001 and elastic deformation during indenter indentation (in Russian). Soviet
1002 Physics - Doklady. 26, 769–771.
- 1003 Tabor, D., 1977. Surface forces and surface interactions. J. Colloid Interface
1004 Sci. 58 (1), 2–13.
- 1005 Wahl, K. J., Asif, S. A. S., Greenwood, J. A., Johnson, K. L., 2006. Oscillat-
1006 ing adhesive contacts between micron-scale tips and compliant polymers.
1007 J. Colloid Interface Sci. 296, 178–188.
- 1008 Wieckiewicz, M., Grychowska, N., Zietek, M., Wieckiewicz, W., 2016. Eval-
1009 uation of the elastic properties of thirteen silicone interocclusal recording
1010 materials. BioMed Research International. 2016, 7456046.
- 1011 Yu, Y., Sanchez, D., Lu, N., 2015. Work of adhesion/separation between soft
1012 elastomers of different mixing ratios. J. Mater. Research. 30 (18), 2702–
1013 2712.

1014 **Appendix A. The results of application of the BG method (com-** 1015 **plete set)**

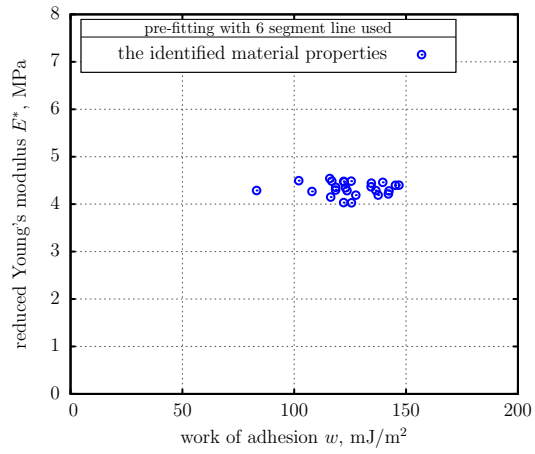
1016 In the following figures the results of identification of the PVS properties
1017 are shown as the number of segments in the pre-fitting polygonal chain varies
1018 from 4 to 10. The values of E^* and w were identified separately for each of
1019 the 25 data sets. The result of each identification is represented as a dot in
1020 the figures.



(a)

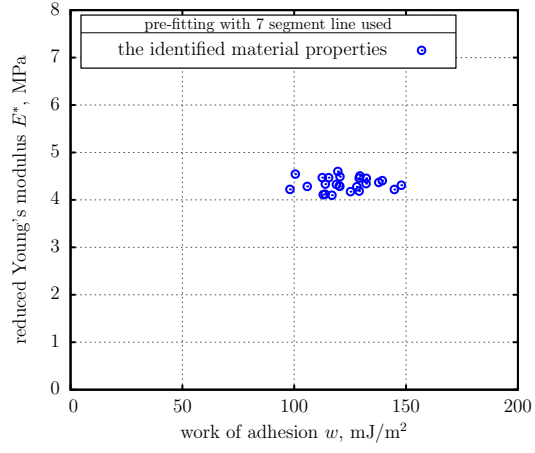


(b)

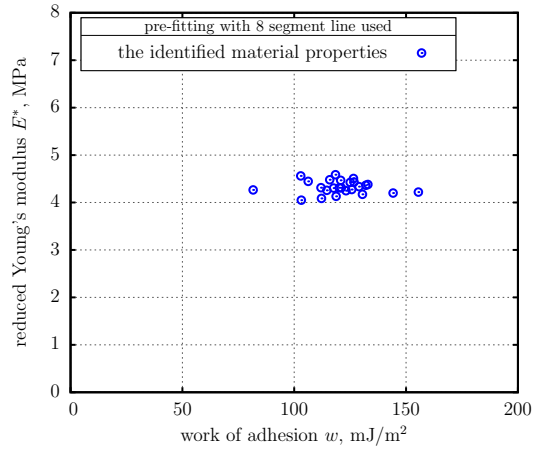


(c)

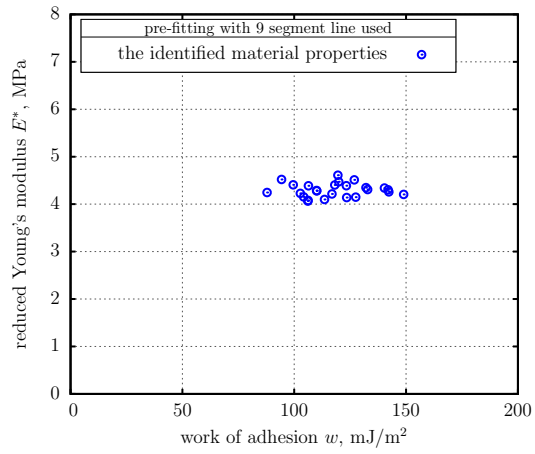
Figure A.19: Material properties extracted using pre-fitting with polygonal chain. Number of segments in chain are correspondingly 4 (a), 5 (b), 6 (c).



(a)



(b)



(c)

Figure A.20: Material properties extracted using pre-fitting with polygonal chain. Number of segments in chain are correspondingly 7 (a), 8 (b), 9 (c).

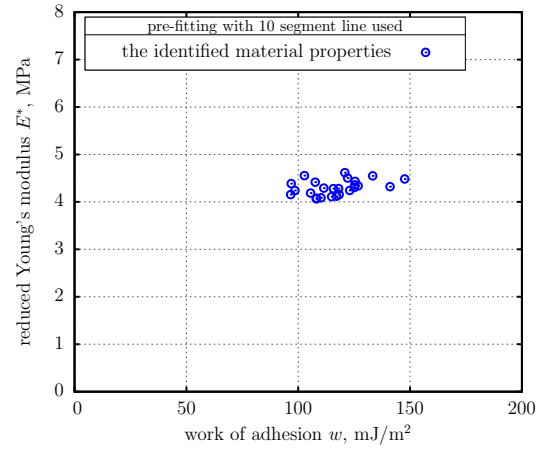


Figure A.21: Material properties extracted using pre-fitting with polygonal chain. Number of segments in chain: 10.